# Very Short Range Local Area Weather Forecasting Using Measurements from Geosynchronous Meteorological Satellites

By

Gerald J. Sikula and Thomas H. Vonder Haar

Department of Atmospheric Science
Colorado State University
Fort Collins, Colorado

Colorado State University

Department of Atmospheric Science

Paper No. 185

AFCRL-72-0260

# VERY SHORT RANGE LOCAL AREA WEATHER FORECASTING USING MEASUREMENTS FROM GEOSYNCHRONOUS METEOROLOGICAL SATELLITES

by

Gerald J. Sikula and Thomas H. Vonder Haar
Department of Atmospheric Science
Colorado State University
Fort Collins, Colorado

Contract No : F19628-71-C-0073
Project No : 6698
Task No : 669802
Work Unit No: 66980201

FINAL REPORT
Period Covered: 1 November 1970 through 31 January 1972

Contract Monitor: John H. Conover, Meteorology Laboratory

30 April 1972



Prepared for
AIR FORCE CAMBRIDGE RESEARCH LABORATORIES
AIR FORCE SYSTEMS COMMAND
UNITED STATES AIR FORCE
BEDFORD, MASSACHUSETTS

ABSTRACT

Qunatitative radiance measurements from NASA's ATS-3 geosynchronous satellite have been used to develop and test a statistical forecast method to predict air terminal weather over the very short range (0-6 hours) time period. Results from more than 800 hourly weather situations at a wide range of U. S. weather stations show that the parameters of ceiling and total opaque cloud cover can be specified or predicted with skill; exceeding persistence forecasts for time periods greater than two hours. Statistical predictions based on satellite data alone are much better than those based on some 500 mb upper air parameters tested. The potential global applications of the satellite data-based forecasts can apparently be improved by the use of certain criteria, such as region of interest, in developing and applying the multiple regression equation. Considering the present status of objective short range weather forecasting, these first results using geosynchronous satellite data demonstrate a new potential for improved forecasts at this scale.

Gerald J. Sikula*
Thomas H. Vonder Haar
Atmospheric Science Department
Colorado State University
Fort Collins, Colorado 80521
April, 1972

Atmospheric Science Paper No. 185

---

*A portion of this work was initially prepared by this author in partial fulfillment of the requirements for the degree of Master of Science, Atmospheric Science, Colorado State University, 1971.

TABLE OF CONTENTS


| | page |
|---|---|
| ABSTRACT | i |
| TABLE OF CONTENTS | ii |
| LIST OF TABLES | iv |
| LIST OF FIGURES | v |
| LIST OF SYMBOLS | vi |
| 1.0 Introduction | 1 |
| 2.0 Selection and Preparation of Data Set | 4 |
| 2.1 ATS Satellite | 4 |
| 2.2 Selection of ATS Data Set; Satellite Position | 5 |
| 2.3 Selection of Terminals | 7 |
| 2.4 Surface Meteorological Data | 7 |
| 2.5 Upper Air Data | 8 |
| 2.6 ATS Data Processing | 17 |
| 2.7 ATS Basic Level Checks | 18 |
| 3.0 Statistical Processing of Data | 24 |
| 3.1 Normalization Procedure | 24 |
| 3.2 Statistical Regression Scheme | 28 |
| 3.3 Experiment Design and Tests | 30 |
| 4.0 Analysis of Data | 36 |
| 4.1 Experiment Results | 36 |
| 4.2 Other Results | 51 |
| 5.0 Tests for Forecasting Significance and Usefulness | 53 |
| 6.0 Conclusions and Recommendations | 55 |
| 7.0 References | 59 |

page

ACKNOWLEDGEMENTS . . . . . 61

APPENDIX A. Bi-directional Reflectance Models . . . . . 62

APPENDIX B. Standardization and Normalization Procedures . . . . . 70

LIST OF TABLES


| Table | | Page |
|---|---|---|
| 2.2-1 | Selected ATS data set and satellite position. . . . . | 6 |
| 2.3-1 | Selected terminals. . . . . | 14 |
| 2.4-1 | Coding system for weather data. . . . . | 16 |
| 2.7-1 | Accepted ATS data set . . . . . | 23 |
| 3.2-1 | Variables used for computing multiple regression equations . . . . . | 29 |
| 4.1-1 | Derived general regression equations. . . . . | 43 |
| 4.1-2 | Derived regression equations for vorticity stratification. . . . . | 45 |
| 4.1-3 | Derived regression equations for terminal stratification. . . . . | 47 |
| A-1 | $\chi(\zeta,\theta,\psi)$ factors for the Nimbus III ocean model . . . . . | 68 |
| A-2 | $\chi(\zeta,\theta,\psi)$ factors for the Nimbus III cloud model . . . . . | 69 |
| B-1 | Directional reflectance relative to the value at solar zenith angle of zero degrees for the Nimbus III ocean and cloud models. . . . . | 72 |

LIST OF FIGURES


| Figure | | Page |
|---|---|---|
| 2.2-1 | ATS III, 17 Mar. 1970, 1904Z. U.S. enlargement. . . . . | 9 |
| 2.2-2 | ATS III, 24 Mar. 1970, 1709Z. Full frame. . . . . | 10 |
| 2.2-3 | ATS III, 28 Apr. 1970, 1559Z. Western U.S. enlargement. . . | 11 |
| 2.2-4 | ATS III, 2 May 1970, 1648Z. Full frame. . . . . | 12 |
| 2.2-5 | ATS III, 11 May 1970, 1737Z. Eastern U.S. enlargement. . . | 13 |
| 2.3-1 | Map showing U. S. air terminals used on the study. . . . . | 15 |
| 2.7-1 | A contour analysis of the digitized reflected radiance over White Sands, New Mexico from ATS III. Time: 11 May 1970, 1916Z Digital range: 0-255 digital count. . . . . | 22 |
| 3.0-1 | Standard grid array about a terminal (solid lines) Experimental grid array (dashed lines) . . . . . | 25 |
| 3.1-1 | A simplified block diagram of the major steps of data processing. . . . . | 27 |
| 4.1-1 | Graphical display of results of the general regression experiments; contrast with persistence . . . . . | 43 & 44 |
| 4.1-2 | Graphical display of results of regression experiments over midwest United States terminals; contrast with persistence. . . . . | 48 |
| 4.1-3 | Graphical display of results of regression experiments over northeast United States terminals; contrast with persistence. . . . . | 49 & 50 |
| 5.0-1 | RMS error of statistical forecasts using satellite data compared to forecast error in results based on climatology (MAD) and on persistence ($RMS_p$) . . . . . | 56 |
| A-1 | Geometry of reflectance. . . . . | 63 |
| A-2 | Vertical cross-section through the $\chi$ model for the ocean depicting the difference in reflective characteristics between a Lambert surface and the observed ocean. $\zeta = 35°\text{-}60°$, $\theta = 20°\text{-}30°$, $\psi = 0°\text{-}180°$. . . . . | 66 |
| A-3 | Vertical cross-section through the $\chi$ model for a cloud depicting the difference in reflective characteristics between a Lambert surface and observed clouds. $\zeta = 35°\text{-}60°$, $\theta = 40°\text{-}50°$, $\psi = 0°\text{-}180°$ . . . . . | 67 |

## LIST OF SYMBOLS

### English Letters

| | |
|---|---|
| $\overline{B}$ | mean brightness |
| D | digital count of brightness |
| H | average height of 500 mb surface |
| $H_i$ | incident solar irradiance |
| K | constant of proportionality |
| N | number of cases |
| $N_r$ | measured effective solar radiance |
| r | directional reflectance |
| R | coefficient of linear multiple correlation |
| S | standard error of estimate |
| T | average temperature at 500 mb |
| UU | average west wind component at 500 mb |
| V | baroclinic vorticity |
| VV | average south wind component at 500 mb |
| $V_o$ | voltage output from the ATS III camera |
| Z | Greenwich mean time |

### Greek Letters

| | |
|---|---|
| $\zeta$ (zeta) | solar zenith angle |
| $\eta$ (eta) | correction factors used during standardization and normalization |
| $\theta$ (theta) | satellite zenith angle |
| $\mu$ (mu) | micrometer |
| $\rho$ (rho) | bi-directional reflectance |
| $\sigma$ (sigma) | standard deviation |
| $\chi$ (chi) | anisotropic factor |
| $\psi$ (psi) | relative solar azimuth angle |
| $\psi_1$ | solar azimuth angle |
| $\psi_2$ | satellite azimuth angle |
| $\Omega$ (omega) | solid angle |

## 1.0 Introduction

The purpose of this study is to investigate the usefulness of geosynchronous metecrological satellite data as an aid to short-term weather forecasting. Since short-term (1-6 hours) weather phenomena often critically affect aircraft operations and other modes of transportation, agriculture and additional industries, as well as the general public, their predictability is a valid scientific goal. The Committee on Atmospheric Sciences (1971) of the National Academy of Sciences lists "short-period extrapolations of local weather" second only to the Global Atmospheric Research Program in its recommendations and priorities for the future.

Lorenz (1969) has recently demonstrated that for cumulus scale features (40 km) the physical equations which govern the atmosphere are limited to approximately one hour of predictability. Beyond this critical time, the small errors inherent in the initial data grow to such an extent that they make worthless any forecast beyond the critical one hour period. Over longer time periods (12 hours and greater) some success has been reported by physical-numerical mesoscale models (Hadeen, 1971). The present study is designed to reduce the void in objective forecasting on the 1-6 hour time scale.

In addition, an important goal of this study is to allow the objective forecasts to be made in normally data-void or "blind" areas. This possibility arises solely because of the recent availability of high-resolution measurements from geosynchronous satellites (data from NASA's ATS-3 are used in the present study). Thus, based on nearly continuous views of the developing and advecting weather features (as noted by clouds), the results of this study demonstrate a potential

for global application independent of a supporting network of surface observations.

In recent years, a statistical approach to short-term forecasting has proven to be at least partially successful. Using multiple regression equations, a series of predictors are statistically screened to yield a best fit towards the dependence of a desired predictand. The resultant regression equation may then be used for predicting a desired weather phenomenon (predictand) as a function of the values of other meteorological parameters (predictors). For example, Keaty and Allen (1970) have reported a regression technique for forecasting low categories of ceiling and visibility via similar surrounding observations as predictors. The National Meteorological Center (NMC) has operationally applied a set of multiple regression equations for predicting maximum and minimum surface temperatures from other conventional meteorological parameters (Klein and Lewis, 1970). In many cases the statistical techniques allow the prediction of weather variables based on the observed or predicted circulation parameters. Furthermore, centrally-prepared dynamical-statistical forecasts provide local area prediction guidance free of unknown biases encountered in centrally prepared man-machine mix forecasts.

Satellite measured reflected radiance (brightness) values are new predictors that are physically related to and may correlate well with such surface parameters as total cloud cover, ceiling, visibility and possibly others. This new type of information may be a vital one in the development of better short-term statistical forecasts. It is the purpose of this study to quantitatively investigate this possibility. In

a pilot study, Vonder Haar and Cram (1970) developed the basic ideas and techniques of using ATS satellite data toward short-term terminal forecasting. Therefore, a portion of this present study is based upon the results of that earlier pilot study.

## 2.0 Selection and Preparation of Data Set

Prior to the actual use of any large amount of data, a number of preliminary procedures and checks are required. In the case of experimental satellite data, these procedures should not be underestimated. The signal received by the satellite and available for research is an analog representation of the response of the sensor to a surface whose exact location is usually approximated by ±10 nm (nautical mile). Obviously, the limitations of this "raw signal" are unacceptable to detailed scientific research. Therefore, it presently is mandatory to use several intermediate procedures to convert the "raw signal" into acceptable scientific data.

After a background section on the ATS satellite, the major steps in the selection and preparation of the data are presented. Each of these sections is only a brief review and, consequently, the intrigued reader is referred to the references.

### 2.1 ATS Satellite

NASA's experimental Applications Technology Satellites (ATS) 1 and 3 have provided earth pictures since their launches on December 7, 1966 and November 5, 1967, respectively. These geostationary satellites have added a new dimension to the field of meteorology in that man now has the capability of observing the short-time changes (approximately 30 minutes) of weather systems over the majority of the sun-lit hemisphere. At altitudes of 19,320 nm (5.6 earth radii) above the earth's equator, both satellites were engineered to obtain high precision measurements of reflected solar radiation from spots on the earth as small as 2 nm (Suomi and Parent, 1968, Suomi and Vonder Haar, 1969).

Although ATS III was designed to provide color earth pictures, a malfunction in the red channel resulted in the use of only the green channel (0.48-0.58μ) to produce black and white earth pictures. During the spring of 1970, the satellite was positioned between 85° and 60° West longitude, affording the spin-scan camera on board a good view of the United States. This spin-scan camera, actually a set of photo-multiplier tubes behind a small Cassegrainian telescope, measured reflected solar radiance as it scanned the earth's disc. West-to-east scans resulted from spacecraft rotation (nominally 100 rpm), while north-to-south scans were accomplished by mechanical stepping. The voltage output of the ATS spin-scan camera is directly proportional to the reflected radiance (Vonder Haar, 1969) from the camera's field-of-view (0.1 milliradians).

After transmission to NASA's ground station at Rosman, N. C., the ATS data are video-processed and stored in analog form on magnetic tape. These tapes are then sent to the Space Science and Engineering Center (SSEC) at the University of Wisconsin for use and archiving.

## 2.2 Selection of ATS Data Set; Satellite Position

All of the satellite data used in this study were obtained from the multicolor spin-scan cloud camera onboard NASA's experimental ATS III satellite. The primary factor in the selection of data days was the availability of taped ATS III satellite data over a long time sequence (approximately two days). In addition, the requirement to view active weather patterns over the United States centered the period of interest to the winter and spring of 1970. Active weather patterns were associated with mid-tropospheric troughs and significant vorticity advection at 500 mb. A third requirement was that the final data set be large

enough such that project results would be statistically significant even after sub-division into various categories.

Under these three basic criteria, 12 days were selected to compose the ATS data set. These 12 days, which are shown in Table 2.2-1, are only a limited sample of weather phenomena, but were purposely chosen to encompass a transition season such that project results would be less dependent upon one particular season.

Table 2.2-1

Selected ATS data set and satellite position

| Day (1970) | Number of pictures | Data time (Z) | ATS III sub-longitude (°W) |
|---|---|---|---|
| March 15 | 5 | 1513-1816 | 83.3 |
| March 16 | 1 | 1504 | 83.1 |
| March 17 | 7 | 1433-2037 | 82.9 |
| March 18 | 7 | 1456-2036 | 82.7 |
| March 24 | 5 | 1435-1830 | 81.4 |
| March 25 | 5 | 1626-2038 | 81.2 |
| April 27 | 6 | 1446-2028 | 74.8 |
| April 28 | 6 | 1432-1947 | 74.6 |
| May 2 | 6 | 1439-1921 | 73.9 |
| May 3 | 4 | 1420-1656 | 73.7 |
| *May 11 | 14 | 1422-2209 | 72.4 |
| May 12 | 4 | 1509-1742 | 72.3 |
| Total | 70 | | |

*May 11, 1970, the day of the Lubbock, Texas tornadoes, has seven pictures with an approximate 20 minute time increment.

Although the ATS III satellite drifted at the rate of 0.1 to 0.2 degrees longitude per day, it is assumed to be geostationary (at 35,770 km above the earth's equator and respective sub-longitude) during the picture taking portion of each day. Several examples of the selected ATS data are shown in Figure 2.2-1 through Figure 2.2-5 in image form. Many high resolution reflected radiance arrays and analyses are contained in the pilot study by Vonder Haar and Cram (1970), (see also Figure 2.7-1).

## 2.3 Selection of Terminals

In order to sample a wide variety of local climatological effects and to observe how these factors might affect the correlation between surface weather and radiance values, 15 stations were chosen across the United States. The 15 terminals, location, and local noon of each are given in Table 2.3-1. Figure 2.3-1 depicts the selected terminals on a standard U. S. map.

## 2.4 Surface Meteorological Data

Copies of WBAN Form A and B (surface weather observations) for the winter and spring of 1970 were obtained from the National Climatic Center. For each of the 15 stations, seven categories of observed weather parameters were encoded as shown in Table 2.4-1.

Several of these weather parameters are non-linear and occasionally discontinuous in nature. However, it was assumed that in the first approximation, a simple linear relationship was a good basis for this preliminary research study. Since the ATS data are nominally available

between 1500Z and 2100Z, the surface reports were encoded between 1200Z and 0300Z to allow for some overlap and permit a maximum of six hour forecast verification.

## 2.5 Upper Air Meteorological Data

Mean daily values of wind, temperature, height and baroclinic vorticity were obtained from the National Meteorological Center's (NMC'S) 500 mb. analysis fields by averaging the 1200Z and 2400Z values of each parameter over each station. The mean 500 mb. wind vectors were further reduced to their scalar components of average west wind (UU) and average south wind (VV) which resulted in five upper air parameters of AVGUU, AVGVV, AVGT, AVGH and AVGV. These averaged upper air data were used in various subsequent experiments as stratification criteria and secondly, as independent variables in the multiple regression equations.

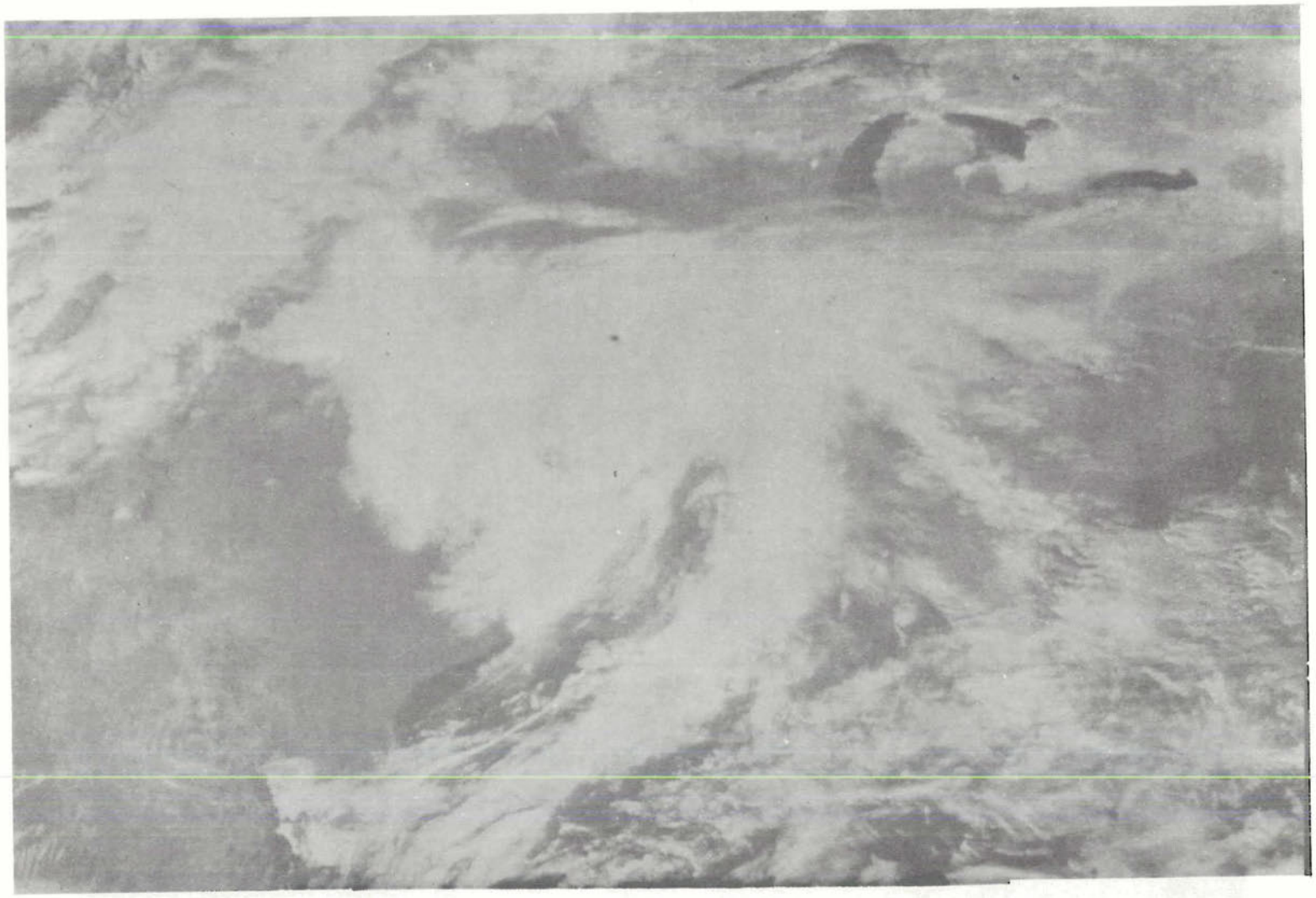

Figure 2.2-1 ATS III, 17 Mar. 1970, 1804Z.
U.S. enlargement.

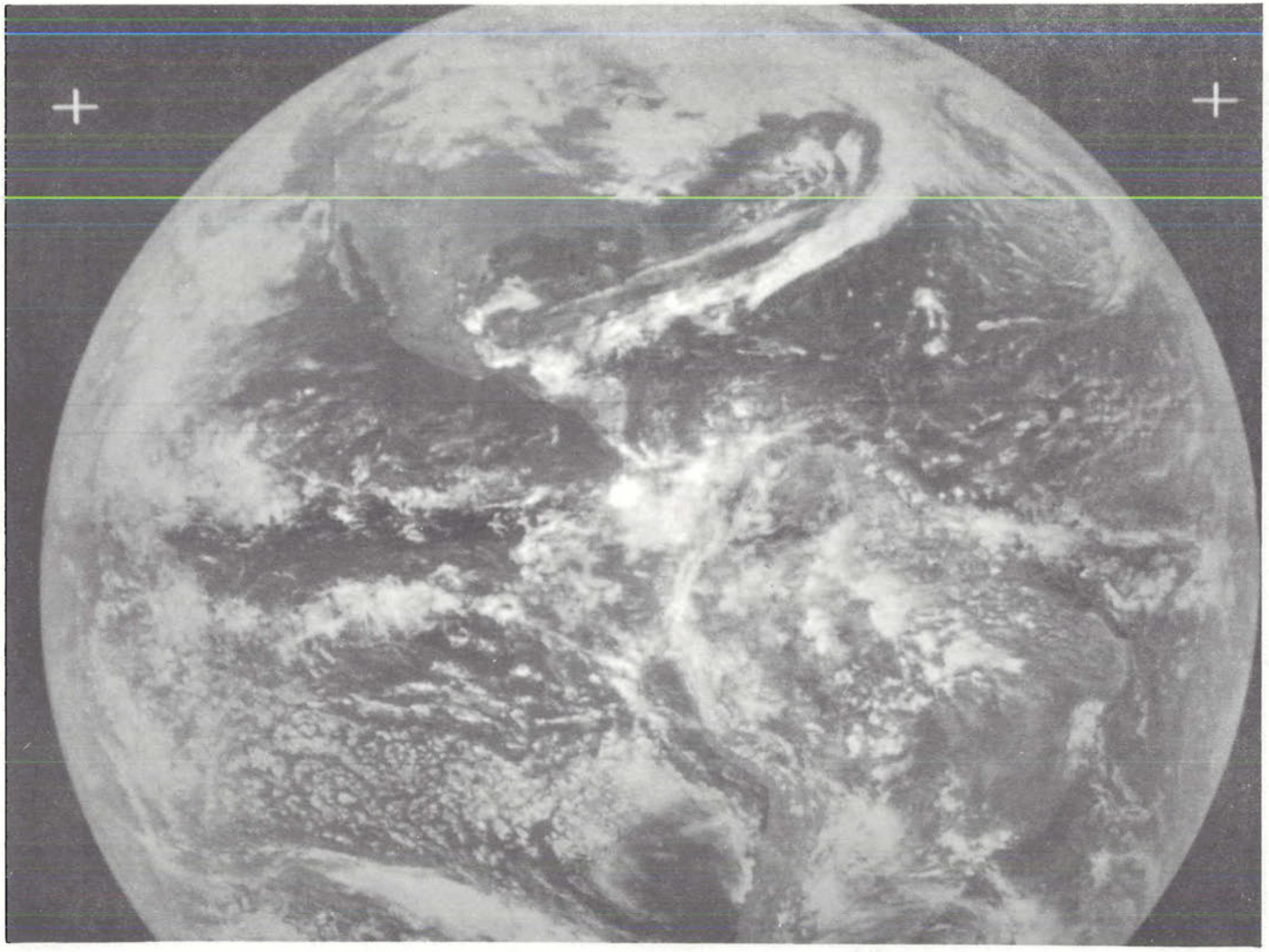

Figure 2.2-2 ATS III, 24 Mar. 1970, 1709Z
Full frame.

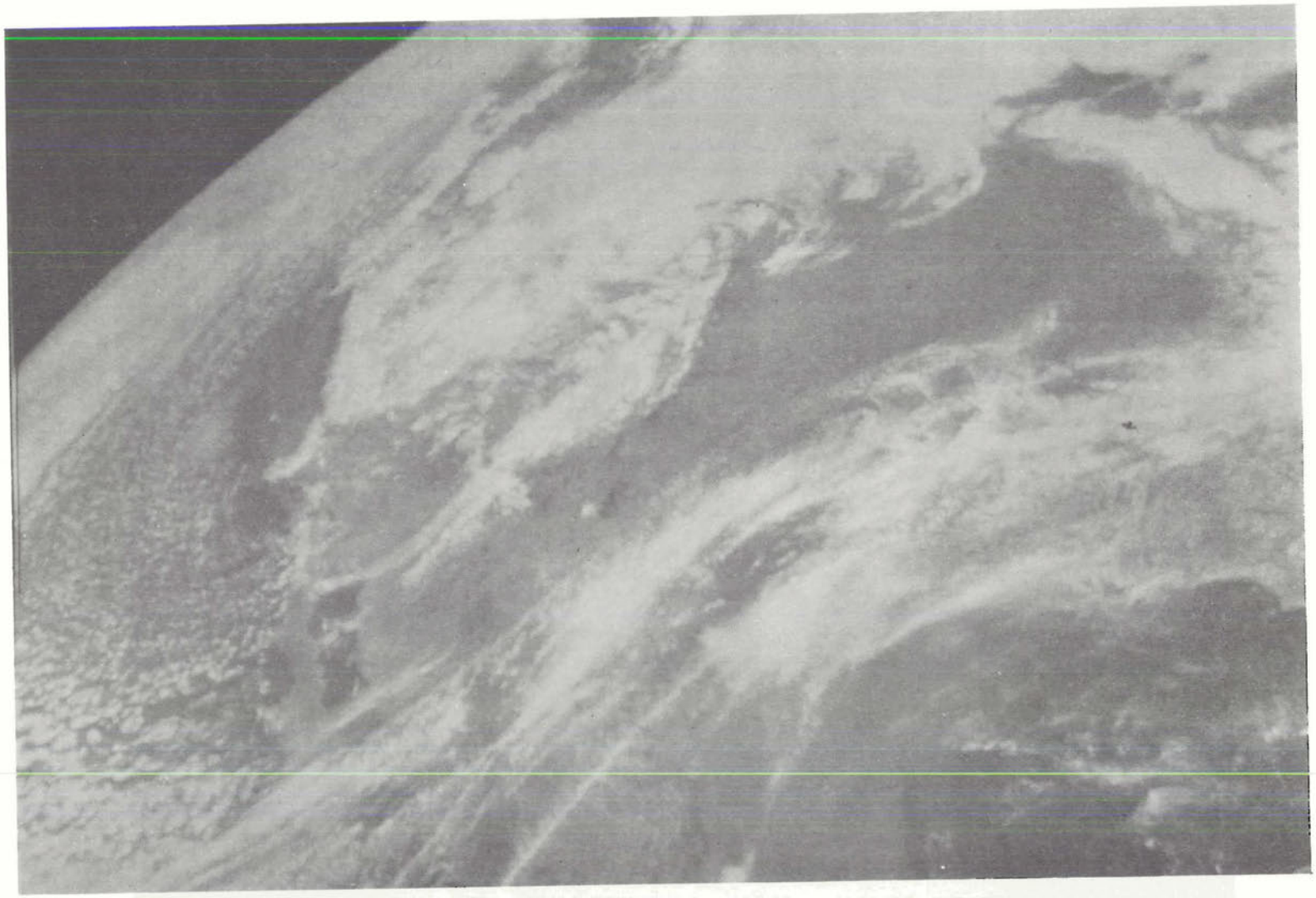

Figure 2.2-3 ATS III, 28 Apr. 1970, 1559Z.
Western U.S. enlargement.

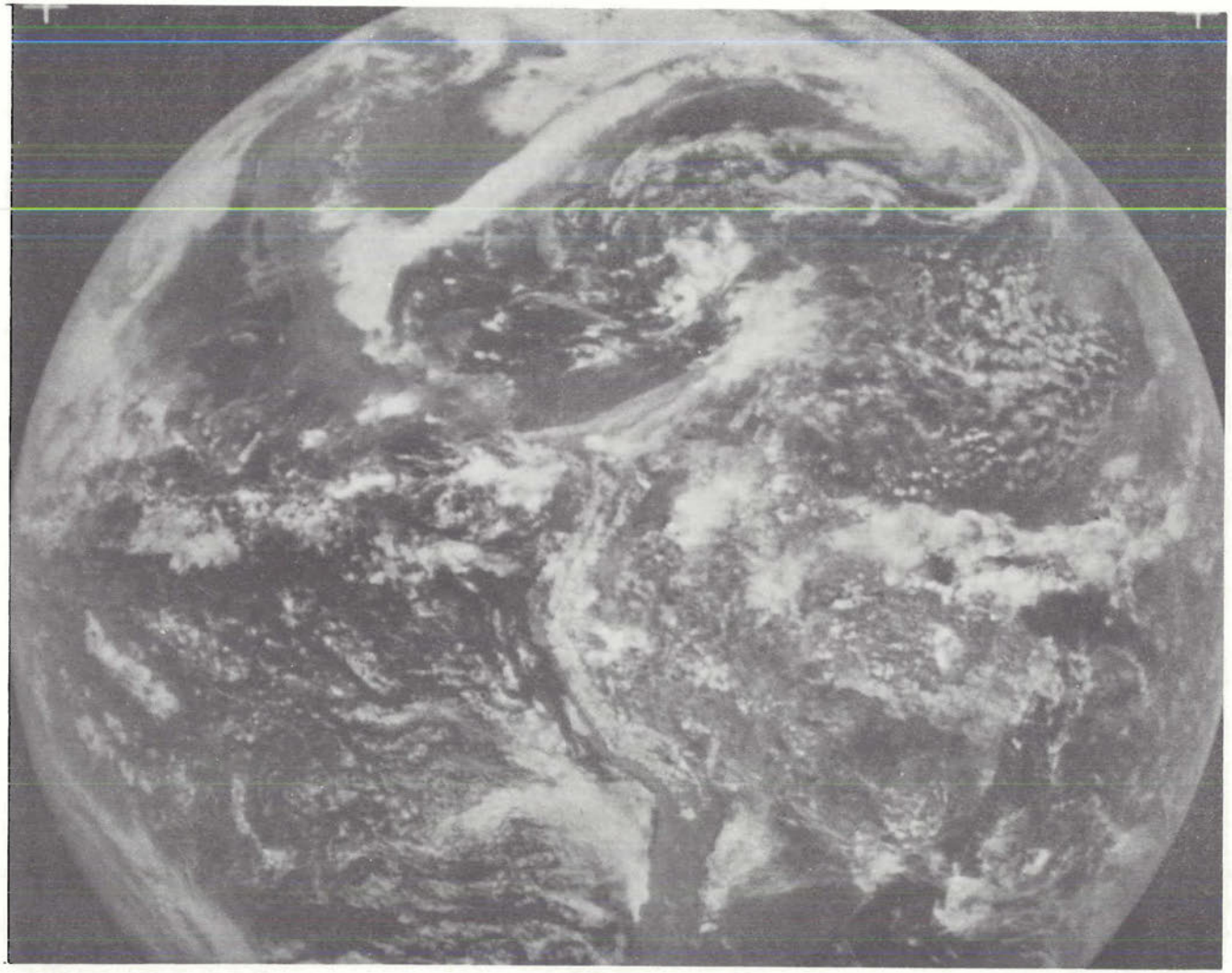

Figure 2.2-4 ATS III, 2 May 1970, 1648Z.
Full frame.

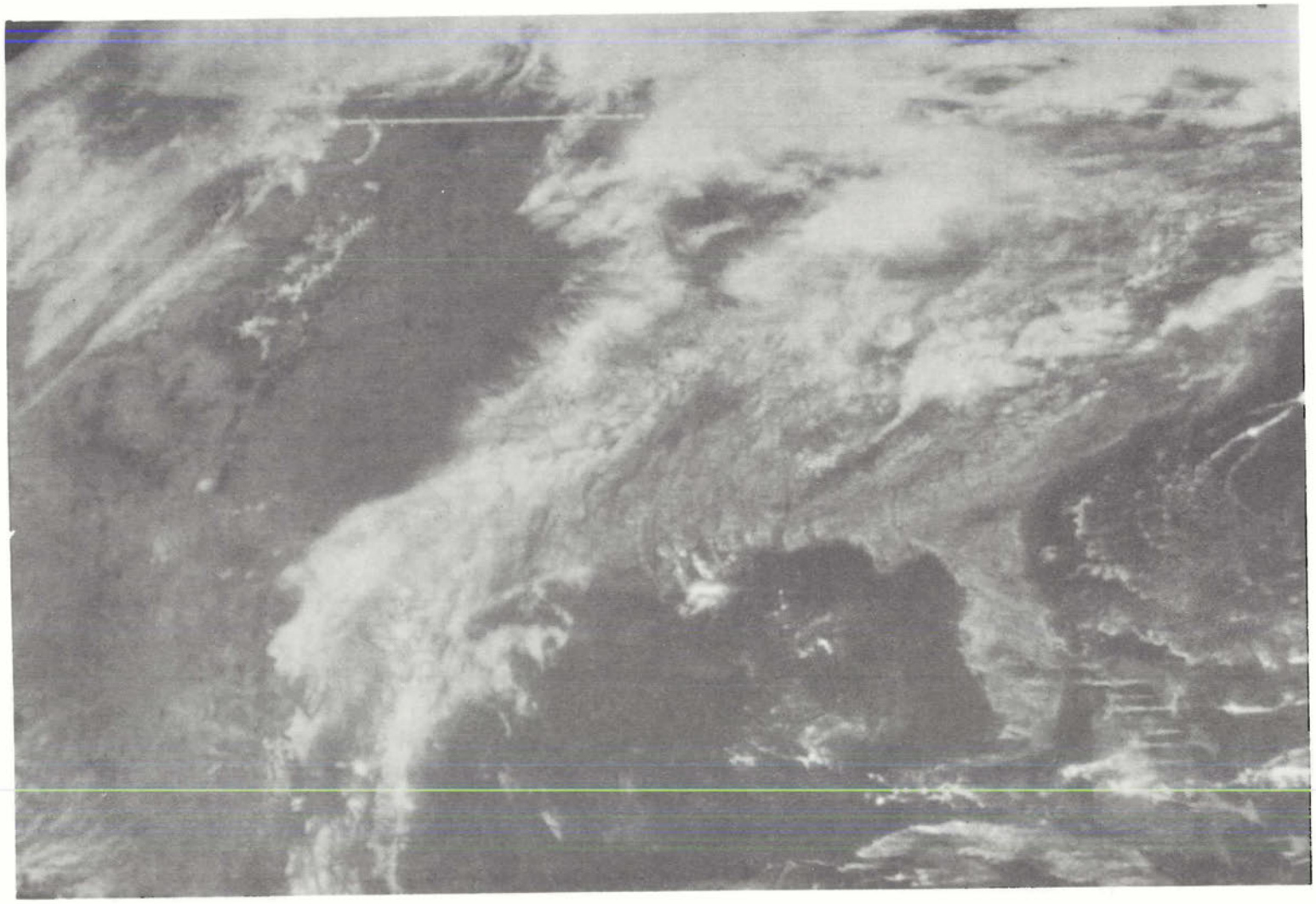

Figure 2.2-5 ATS III, 11 May 1970, 1737Z.
Eastern U.S. enlargement.

Table 2.3-1

Selected terminals

| Terminal | Identifier | Latitude (°N) | Longitude (°W) | Local noon (Z) |
|---|---|---|---|---|
| 1. Albany, N. Y. | ALB | 42.747 | 73.805 | 1655 |
| 2. Atlanta, Ga. | ATL | 33.642 | 84.426 | 1738 |
| 3. Washington, D. C. | DCA | 38.852 | 77.038 | 1708 |
| 4. Denver, Colo. | DEN | 39.765 | 104.880 | 1900 |
| 5. LaGuardia, N. Y. | LGA | 40.777 | 73.873 | 1655 |
| 6. Los Angeles, Calif. | LAX | 33.942 | 118.407 | 1954 |
| 7. North Platte, Neb. | LBF | 41.128 | 100.696 | 1843 |
| 8. New Orleans, La. | MSY | 29.992 | 90.255 | 1801 |
| 9. Omaha, Neb. | OMA | 41.300 | 95.893 | 1824 |
| 10. Chicago, Ill. | ORD | 41.983 | 87.907 | 1752 |
| 11. San Antonio, Tex. | SAT | 29.531 | 98.470 | 1834 |
| 12. San Francisco, Calif. | SFO | 37.619 | 122.376 | 2010 |
| 13. Springfield, Mo. | SGF | 37.244 | 93.387 | 1814 |
| 14. Salt Lake City, Utah | SLC | 40.784 | 111.967 | 1928 |
| 15. Tulsa, Okla. | TUL | 36.198 | 95.890 | 1824 |

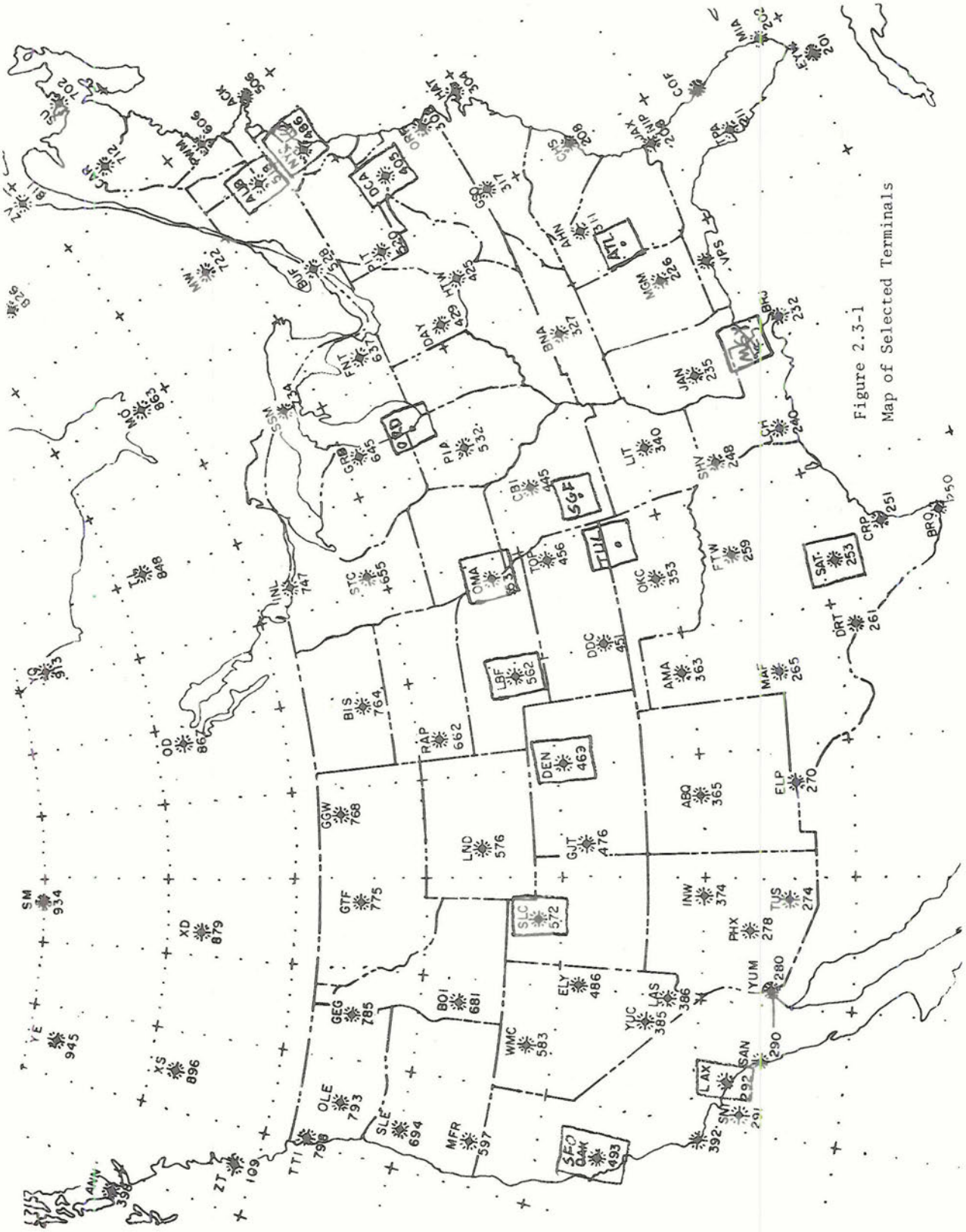


Figure 2.3-1 Map of Selected Terminals

TABLE 2.4-1

CODING SYSTEM FOR WEATHER DATA

| | Parameter | Range | Explanation |
|---|---|---|---|
| 1. | Ceiling | 000-400 | Ceilings were encoded in hundreds of feet. Scattered clouds = 350 and clear skies = 400. In the absence of a ceiling, a partial surface obscuration was encoded 010 and a total obscuration = 005. U (undetermined height) = 300. |
| 2. | Visibility | 00.00-15.00 | Recorded in statute miles. |
| 3. | Sea level pressure | 0900.0-1030.0 | Recorded in millibars. |
| 4. | Weather and obstructions to vision | 00-10 | If two or more phenomena were simultaneously observed, only the highest code was recorded according to the following:<br>10 = Thunder, thunderstorm;<br>09 = (blank)<br>08 = Rain shower, snow shower;<br>07 = (blank)<br>06 = Rain, sleet, snow;<br>05 = Drizzle;<br>04 = Fog;<br>03 = Dust, sand;<br>02 = Haze;<br>01 = Smoke;<br>00 = None reported |
| 5. | Step function of weather and obstructions to vision | 00-03 | 03 = Thunder, thunderstorm;<br>02 = Rain shower, snow shower, rain, sleet, snow;<br>01 = Drizzle;<br>00 = Fog, dust, sand, haze, smoke, none reported. |
| 6. | Total cloud amount | 00-10 | Reported in tenths of sky covered by all visible clouds. (The sky or celestial dome seen by a ground observer is approximately 25 nm in diameter). |
| 7. | Total opaque cloud amount | 00-10 | Tenths of sky hidden by clouds through which the sky cannot be seen. |

## 2.6 ATS Data Processing

The ATS radiance values used in the study were obtained from the Space Science and Engineering Center (SSEC) at the University of Wisconsin. Three basic steps of initial ATS data processing, previously designed by Smith, Phillips and Vonder Haar,[1] were accomplished at the SSEC. Each of these is outlined below.

Since ATS data are archived in analog form at the SSEC, the first step is an analog to digital conversion of the ATS radiance values. Digital radiance values between 0 and 255 (eight binary bits) were used to provide a large range of brightness (radiance) values while still permitting a relative ease for computer processing. After digitization, one ATS III earth picture is composed of 2408 scan lines (rows) with 8192 samples (elements) per line.

An intermediate process involves computing ocean brightness statistics which are used for a standardization check of each picture, as discussed in section 2.7.

The second major step involves the navigation or earth-locating of each ATS picture. Recognizable landmarks within each ATS data array are used to derive the orientation of the satellite's spin axis. These derived navigation parameters are then used in conjunction with satellite orbital data in an analytical program to navigate each ATS picture to a best-fit position. The resulting average error in the navigation process is ten nautical miles over the region of interest.

The final step of the SSEC processing involves the rectification of the satellite data from their original latitude and longitude

---

[1] Unpublished report.

positions over the United States to corresponding positions on a rectangular grid of latitude and longitude lines. By averaging data values in low latitudes and interpolating values in higher latitudes, a constant factor of 24 rows of data per degree latitude and 72 columns of data per degree longitude is maintained.[2] Thus, when a certain area of data is needed, the row and column (latitude and longitude) boundaries of that area must be specified.

To minimize data handling and peripheral processing expenses, each digitized, navigated and rectified ATS picture was further limited to approximately 46°-26° N and 127°-67° W (the majority of the contiguous United States).

## 2.7 ATS Basic Level Checks

A number of factors must be accounted for before any comparisons among ATS pictures are possible. The following six factors are responsible for a variation with respect to time of the received satellite signal from a given area even when the satellite position is constant.

1. Changes of the physical characteristics of the viewed cloud such as phase state, size distribution of the condensate, the amount of condensate and cloud thickness.
2. Changes in the observed cloud field due to advection.
3. Cloud anisotropy which may be defined as variations in the angular reflective characteristics of the cloud due to a changing solar hour angle.

---

[2] Digital tapes for the 24th and 25th of March, 1970 used a constant factor of 20 rows per degree latitude and 66 columns per degree longitude.

4. Spacecraft camera gain settings.

5. Spacecraft to ground station telemetry link.

6. Gain settings of the ground receiving and processing equipment.

Relating cloud development and advection to observed surface meteorological parameters is the fundamental goal of this study. However, before any correlations among these parameters are possible, the other factors mentioned above must be minimized or eliminated by preliminary processing.

The third factor, as well as changes in the satellite location, are accounted for through the bi-directional reflectance models which are presented in Appendixes A and B. The last three factors are man-controlled but not always completely recorded. Therefore, a basic level check (henceforth called standardization) was designed to reveal any unrecorded gain settings that would affect later inter-daily data comparisons. A second portion of the basic check (henceforth called White Sands) was designed to eliminate any ATS data that were grossly misaligned during the navigation procedure. Both of these checks are outlined below.

1. Standardization

Part of the initial ATS data processing involved selecting a small cloud-free ocean area (approximately $1^\circ \times 1^\circ$) in the low latitudes of each ATS picture. The clear ocean brightness values (approximately 1500/area) were used to compute a mean brightness ($\bar{B}$) for each ocean spot. Knowing the location of each clear ocean area and the respective earth, sun, satellite geometry, an ocean reflectance model was used to obtain correction factors ($\eta$) for each digitized picture. See

Appendixes A and B for details. Under the five basic assumptions of the standardization procedure, all the reflectance geometry was accounted for via $\eta$; thus, any differences in $\bar{B}$ were a result of different gain settings used during data reception and processing or low level instrument noise.

The five basic assumptions of standardization were:

a. The manually selected ocean areas were actually void of clouds.

b. The ocean reflectance model used was representative.

c. The different tropical ocean areas used had a similar albedo.

d. Ocean waves were not significantly large to affect the albedo.

e. The albedo of the cloud-free atmosphere was similar for all standardization data.

All times and locations were standardized to local noon on 15 April and 30°N, local longitude, which permits a standard solar zenith angle of 20.8°. Furthermore, the ATS III position during the period of interest was standardized to 0°N, 77°W at 35,770 km. altitude.

Computation of $\eta$ indicated corrections averaging 10%. Since the validity of the five standardization assumptions was questionable at this level, the correction factors were not used. This decision was reinforced by the relatively small standard deviation of the original ocean $\bar{B}$'s.[3]

---

[3]The average, mean ocean brightness for standardization was 17.98 units with a standard deviation of 3.76.

The conclusion of the standardization procedure was that the ATS digitized pictures from the chosen period were of such quality of make unnecessary a basic level correction for unrecorded gain settings. Thus, later inter-daily comparisons of digital values were enabled via the standardization check.

2. White Sands

A second portion of the ATS basic check was to manually verify each digitized picture for proper rectification and navigation. Both of these procedures were previously outlined in section 2.5. Utilizing the unique reflectance pattern from White Sands, New Mexico, each of the 70 digitized pictures was checked for its White Sands presentation and location. From these individual checks it was possible to obtain a "best average" location of 32.95°N, 106.38°W for the center of the area of maximum reflectance. One of the better ATS digitized representations of White Sands is shown in Figure 2.6-1.

Since the ATS navigation procedure was limited by an average error of ten nautical miles[4] and furthermore, since the effects of the three principal reflectance angles ($\zeta,\theta,\psi$) upon the location of the area of maximum reflectance were unknown, only the extreme variations of White Sands locus were used to disqualify an ATS picture from further processing. On the basis of a White Sands locus variation of > 30 nm from a "reference position" of 32.90°N, 106.40°W, seven pictures were eliminated. Thus, the accepted ATS data set was established and is shown in Table 2.6-1.

---

[4] An improved navigation procedure with a maximum error of < 5 nm was developed by the SSEC in 1971.

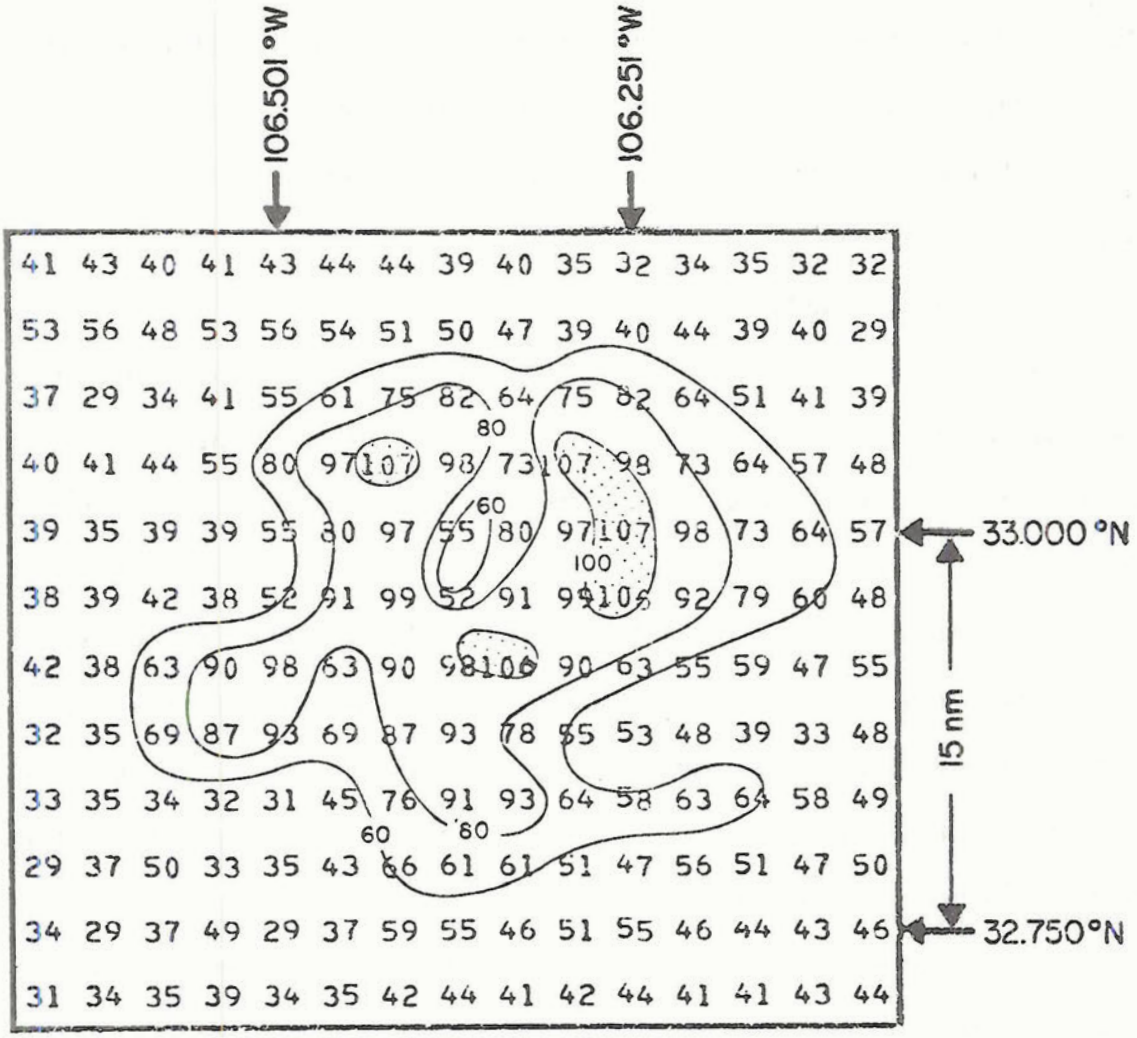


Figure 2.7-1 A contour analysis of the digitized reflected radiance over White Sands, New Mexico from ATS III.
Time: 11 May 1970, 1916Z
Digital range: 0-255 digital count

Table 2.7-1

Accepted ATS data set

| Day (1970) | No. of pictures | Data times (Z) |
|---|---|---|
| 15 March | 5 | 1513, 1605, 1658, 1750, 1816 |
| 16 March | 1 | 1504 |
| 17 March | 7 | 1433, 1532, 1637, 1731, 1837, 1931, 2037 |
| 18 March | 7 | 1456, 1548, 1641, 1759, 1851, 1943, 2036 |
| 24 March | 5 | 1435, 1553, 1645, 1737, 1830 |
| 25 March | 3 | 1626, 1731, 1825 |
| 27 April | 5 | 1446, 1549, 1728, 1802, 2028 |
| 28 April | 4 | 1632, 1739, 1835, 1947 |
| 2 May | 6 | 1439, 1531, 1633, 1737, 1829, 1921 |
| 3 May | 2 | 1512, 1538 |
| 11 May | 14 | 1422, 1538, 1632, 1737, 1832, 1916, 2001, 2023, 2045, 2106, 2128, 2146, 2208, 2229 |
| 12 May | 4 | 1509, 1603, 1658, 1742 |
| Total | 63 | |

## 3.0 Statistical Processing of Data

After the initial ATS data processing of digitization, navigation, rectification and standardization checks, the satellite data were ready for statistical processing about each terminal. Due to the latitude dependence of the length of one degree of the parallel, a standard statistical grid of 60 nm x 50 nm (1° lat. x 1° long. at 34°N) was chosen to be applied at all 15 terminals. This constant area grid, or sub-block, contained approximately 1500 ATS data points and served as the data base from which the ATS brightness statistics were computed. A grid array of nine standard grids was constructed about each terminal with grid number five being centered over the terminal as shown in Figure 3.0-1. Thus, for each ATS data time and about each terminal, nine values per ATS statistic were computed. These ATS statistics were then used as the independent variables from which the multiple regression equations were derived.

An experimental grid size of 30 nm x 25 nm (0.5° lat. x 0.5° long. at 34°N) was used later for special cases to determine its effect. This grid is also displayed in Figure 3.0-1. In addition, several experimental statistics were computed. Further details and a complete listing of the ATS statistics used are given in section 3.2.

## 3.1 Normalization Procedure

Prior to the computation of the ATS brightness statistics, a normalization procedure was applied to the data within the grid array surrounding each terminal. The mid point of each of the nine standard grids within a terminal grid array was used to compute a normalization

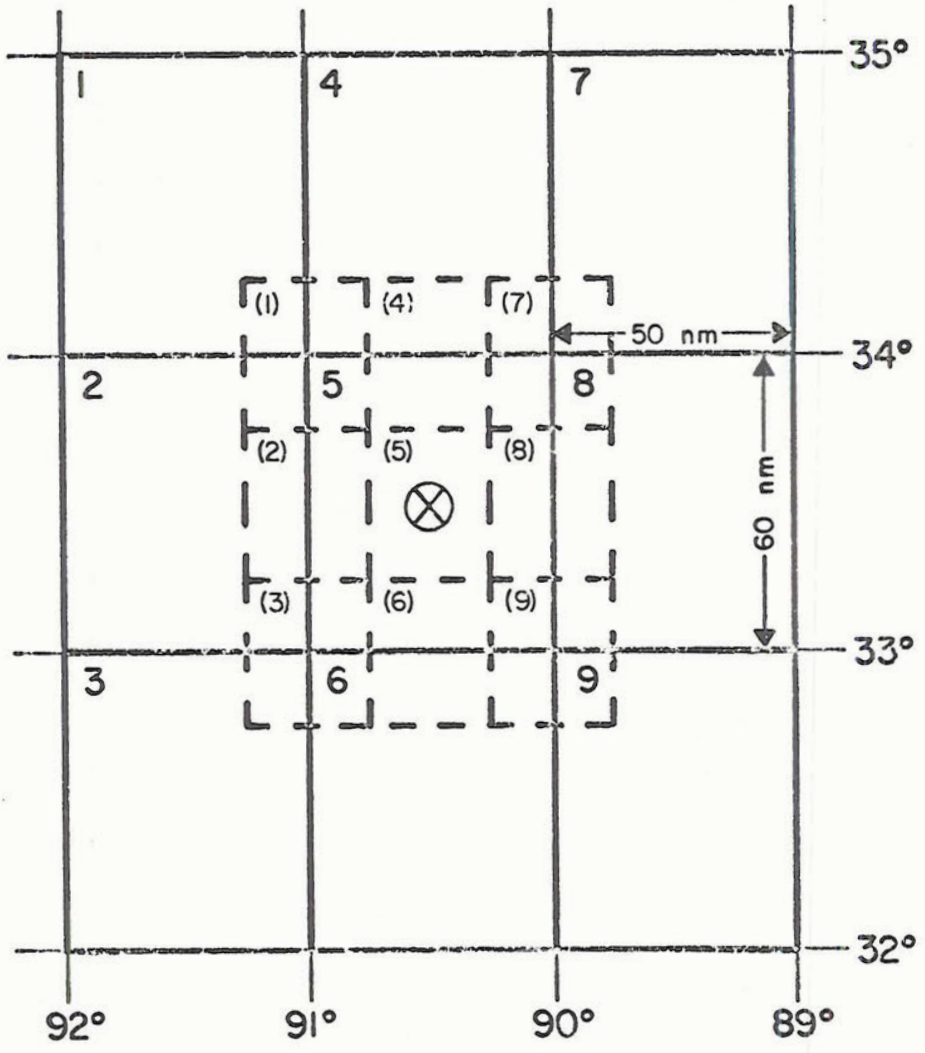


Figure 3.0-1 Standard grid array about a terminal (solid lines). Experimental grid array (dashed lines).

factor, $\eta$, which accounts for cloud anisotropy and changes in incident solar irradiance. Details of the normalization procedure are given in Appendixes A and B. The computed factors vary with terminal location, but in general average 1.90 ± 0.10 near sunrise and sunset, and decrease to a minimum of near 1.00 ± 0.10 at local noon. If a correction factor of $\eta > 3.00$ was computed, these data were not included in further processing. These large $\eta$ values were computed for the 1400Z ATS pictures over the far western United States as a result of the extremely large solar zenith angles ($\zeta$). This limiting value of $\eta$ generally corresponds to limiting the ATS data processing from 0700 LST to 1700 LST, or five hours either side of local noon. The reference time and location for normalization was local noon on 15 April and 30°N, local longitude, while the satellite position was referenced at 35,770 km over 0°N, 77°W. The same technique of computing nine $\eta$'s per terminal grid array was used with the experimental grid size of 30 nm by 25 nm.

As a result of the normalization procedure, relative comparisons of ATS brightness values from clouds could be made. The end result, then, of both the standardization (section 2.7) and the normalization processes was that all of the digital satellite data used during the study were referenced to a common level. Thus, valid relative comparisons could be made, not only on an inter-daily basis, but also at various times within a given day (intra-daily).

Due to the many steps of ATS data preparation involved prior to the actual computation of the multiple regression equations, a brief summary of the major processing procedures is given in Figure 3.1-1.

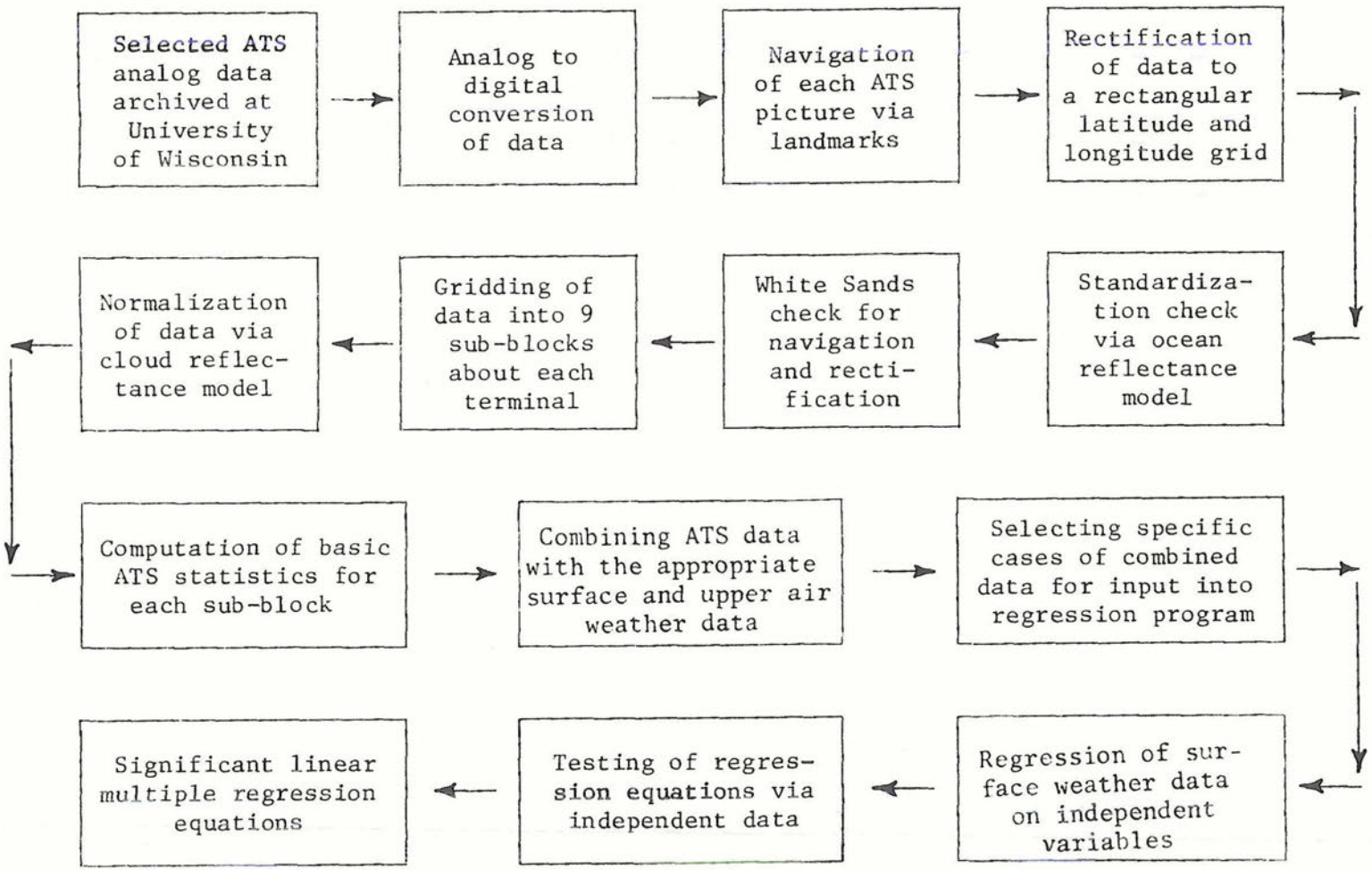


Figure 3.1-1 A simplified block diagram of the major steps of data processing.

## 3.2 Statistical Regression Scheme

A stepwise, least squares, multiple linear regression program was employed to provide the "best" multiple regression equation (MRE) for each dependent variable. The basic stepwise regression program was developed at U.C.L.A. (Dixon, 1970) and later slightly modified by the Statistical Laboratory at Colorado State University. In practice, the program computes a sequence of MRE's in a stepwise manner. At each step, a new independent variable (the one which makes the greatest reduction in the error sum of squares) is added to the regression equation. No attempt was made to investigate the non-linear relationships during this first study. Furthermore, no transgenerations of independent variables were used. Throughout the regression programs the F-level for including an independent variable was adjusted such that entering variables were significant at a minimum of the 95% confidence level. Further details on the technique of computing MRE's may be found in Draper and Smith (1966).

The dependent and independent variables used for MRE computation are shown in Table 3.2-1. The dependent variables (predictands) of observed surface weather parameters for each terminal were used individually with the independent variables (predictors). In this manner a linear regression equation was developed for each dependent variable used. For each satellite independent variable listed, nine values were computed corresponding to the nine standard grids, or sub-blocks, surrounding each terminal.

Table 3.2-1

VARIABLES USED FOR COMPUTING MULTIPLE REGRESSION EQUATIONS

| Dependent variables | Independent variables |
|---|---|
| Ceiling (CLG) | Mean grid brightness ($\overline{B}_i = MN_i$) $i = 1, 2, 3, \ldots 9$ |
| Visibility (VSBY) | Standard deviation of mean grid brightness ($\sigma_{\overline{B}_i} = SD_i$) |
| Sea level pressure (SLP) | Coefficient of variation ($\sigma_{\overline{B}_i} / \overline{B}_i = CV_i$) |
| Weather and obstructions to vision (PRE) | Variance of mean grid brightness ($(\sigma_{\overline{B}_i})^2 = VAR_i$) |
| Step function of weather and obstructions to vision (CIP) | Change of mean grid brightess during the past 60 ±10 min. ($\Delta\overline{B}_t = \overline{B}_{i,t} - \overline{B}_{i,t-1} = DMT_i$) |
| Total cloud amount (TCA) | |
| Total opaque cloud amount (TOCA) | Deviation between mean grid brightness and mean array brightness ($\Delta\overline{B}_{i,d} = \overline{B}_i - \overline{\overline{B}} = DMD_i$) |
| | Average 500 mb west wind (AVG UU) |
| | Average 500 mb south wind (AVG VV) |
| | Average 500 mb temperature (AVG T) |
| | Average 500 mb baroclinic vorticity (AVG V) |
| | Average 500 mb height (AVG H) |
| | A priori ceiling (APCLG) |
| | A priori visibility (APVSBY) |
| | A priori total opaque cloud amount (APTOCA) |

## 3.3 Experimental Design and Tests

The total accepted ATS satellite data set consisted of 63 digitized pictures over the majority of the United States as shown in Table 2.6-1. Using the 15 terminals given in Table 2.3-1, approximately 900 cases covering a wide range of synoptic conditions and terrain features were available for experimentation.

Several experiments were designed to examine techniques of data processing and grouping which would yield the most informative results Obviously, many other tests and arrangements were possible, but these were designed to aid subsequent interpretation in the present study and to give future investigators an indication of which procedures should be more productive. The results of each experiment were expressed in terms of a linear multiple regression equation (MRE) as explained in section 3.2.

A number of methods were utilized to indicate which resulting regression equations were the most useful from both a statistical and a meteorological viewpoint. One statistical measure of "usefulness" is $R$, the coefficient of linear multiple correlation. The product $100\ R^2$ was used extensively as a statistical indication of the percentage of total variation about the mean explained by the linear regression equation (Draper and Smith, 1966). $R^2$ in this study will be termed the reduction of variance:

$$R^2 = \frac{\Sigma(\hat{Y} - \overline{Y})^2}{\Sigma(Y - \overline{Y})^2} \qquad (1)$$

Another statistical test used was the standard error of estimate, $S$, which is a measure of the residual scatter about the regression:

$$S = \frac{(Y - Y)^2}{N - 2}^{\frac{1}{2}} \qquad (2)$$

Meteorologically, significant statistical results were tested with random independent data (approximately 10% of the total data set) that were not used for MRE derivation (see section 5.0). In line with the goals of this research, predictions resulting solely from the use of geosynchronous satellite are emphasized. However, since large scale upper air data (i.e., 500 mb heights, temperatures and vorticity) may also be inferred on a global scale from radiometric temperature sounding experiments on satellites some results are included that use these data as predictors in combination with the primary geosynchronous satellite radiance predictors.

The principal results of each experiment are outlined in section 4.1. An overview of each basic experiment is given below:

Experiment 1 -- Best Variables. The best combination of dependent variables (predictands) and independent variables (predictors) was investigated from the list of all possible variables given in Table 3.2-1. Predictands of ceiling and visibility were considered to be the main goal of the study since they are commonly used in operational weather forecasts. For this experiment only, all of the satellite and surface measured parameters were correlated with each other.

Experiment 2 -- Grid Size. The standard grid size ($1^{o}$ x $1^{o}$) was contrasted with a smaller experimental grid ($0.5^{o}$ x $0.5^{o}$), both of which are shown in Figure 3.0-1. The experimental grid distance of approximately 25 nm of similar to the areal coverage (celestial dome) of the

majority of surface weather observations. Since lag times (experiment 3) of up to six hours were investigated, the primary grid used for the remaining experiments was the standard grid which allowed for more advection.

Experiment 3 -- General Equations and Lag Times. Following the completion of preliminary experiments 1 and 2, several general regression equations were derived for all terminals and all data times. Each general MRE related a chosen predictand to the significant ATS predictors and made no distinction for synoptic situation or terminal location. Later experiments were designed to improve upon the general results of experiment 3 by establishing stratification criteria for meteorological events and geographic effects.

Four different lag times were investigated with most experiments, where lag time is defined as the time of surface weather data minus the time of the ATS data. For example, a 2 hour lag time was used to determine the usefulness of 1600Z ATS data statistics toward forecasting the 1800Z surface weather parameters. Since the satellite data were not measured on the hour, the best time-fit between the satellite and surface data had an occasional maximum time difference of 30 minutes. The four different time lags used were 0, 2, 4 and 6 hours.

Experiment 4 -- Upper Air Predictors. The general regression equations resulting from experiment 3 were derived by using only the ATS parameters as independent variables. Experiment 4 was designed to investigate the usefulness of additional independent variables that would commonly be available from upper air analysis or prognostic fields.

As discussed earlier in section 2.5, five values of mean upper air parameters were obtained over each terminal on each ATS data day. These five additional independent variables are indicated in Table 3.2-1 as the average 500 mb predictors. Thus, the new regression equations would demonstrate the importance and usefulness of typical mid-tropospheric parameters when used for forecasting surface-observed weather phenomenon.

Experiment 5 -- Vorticity and Wind Stratification. In recent years, the vorticity (V) charts produced by the National Meteorological Center (NMC) have played an increasing role in weather forecasting, primarily because of their depiction of trough and ridge passage and related weather developments. In an attempt to improve upon the general equations of experiment 3, a meteorological criterion of vorticity advection was chosen to differentiate between the two broad categories of vertical motion and their associated cloud patterns. Utilizing the baroclinic vorticity charts, three categories of meteorological events were defined by the 12 hour vorticity advection ($\Delta V$) over each terminal, where $\Delta V$ equals the 2400Z forecast vorticity field minus the 1200Z analyzed vorticity field. Category one was positive vorticity advection (PVA), defined by $\Delta V \geq +2$.[5] The mutually exclusive category two was "zero" vorticity advection (OVA), was defined by $\Delta V \leq -2$. The goal of this portion of the experiment was to determine if three equations (dependent upon synoptic features) were significantly more useful than one general equation for all synoptic conditions.

---

[5]The 12 hour vorticity change of ±2 is actually $\pm 2.0 \times 10^{-5}$ $sec^{-1}$ of absolute or total vorticity.

The second portion of experiment 5 was a stratification of the average 500 mb wind direction and speed over each terminal. The average 500 mb winds used for this stratification were obtained by averaging the 1200Z and 2400Z wind vectors over each terminal on each ATS data day, as discussed in section 2.5. Two categories were chosen to delineate between mean westerly advection and mean northwesterly advection. Category one was defined by average 500 mb winds with direction $\geq 240^{o}$ but $\leq 300^{o}$ and speed $\leq$ 30 knots. The second category included 500 mb winds with direction $\geq 301^{o}$ but $\leq 360^{o}$ and speed $\leq$ 40 knots.

The primary goal of the wind stratification was to improve the general equations of experiment 3 for the longer lag times of 4 and 6 hours, by categorizing the mean advection into directional sectors.

Experiment 6 -- Terminal Stratification. This experiment was designed to determine the local and topographical effects upon the general equations of experiment 3. Several sets of data cases were used, the distinguishing features being the number and location of terminals in each set. For example, regression equations were derived for only the west coast terminals to determine if regional equations were significantly more useful than the all-inclusive equations. In addition, individual terminal equations derived by using one terminal and all ATS data times were contrasted with the general equations.

Experiment 7 -- Stratification for Cloud Cases. The reflected radiance measurements of the satellite cloud camera are principally a function of cloud amount in the camera's instantaneous field of view.

During complex meteorological conditions, measured brightness, in addition to conventionally observed weather parameters, might objectively aid the difficult forecasting at these times. Thus, a stratification for cloud conditions was designed to include only those cases where the actual observed ceiling was $\leq$ 20,000 feet at least 50% of the time between 1200Z and 2400Z on the ATS data days. The criterion of 20,000 feet was chosen to limit the effective range of the resulting equations to the lower troposphere and thus enable a more sensitive equations for predicting the lower values of ceiling. Recall that the normal range of the encoded ceiling parameter was 40,000 feet for all other experiments. For this experiment only, the goal was to assess the capability for satellite data in a role supporting the conventional forecasting methods, rather than the capability for forecasting independent of a surface network.

## 4.0 Analysis of Data

Most data were analyzed with the aid of Colorado State University's CDC 6400 digital computer and the stepwise regression computer program (section 3.2). Several data subdivisions, called experiments, were used to test certain aspects of the project. The results of each experiment allowed progress toward more meaningful regression equations. Thus, the remaining sections of this report are devoted to the principal results of each experiment and of the project as a whole.

## 4.1 Experimental Results

The principal results of each basic experiment of section 3.3 are presented below. The discussion is not meant to be complete but only to represent the salient points of each experiment. Although the total data set included approximately 900 cases, most experiments utilized only a portion of the complete set, which is noted as the experimental N (the actual number of cases used). The $R^2$ values quoted in these results were achieved by using two, three, or four ATS predictors. The addition of more independent variables usually increased $R^2$ by less than 0.01.

Experiment 1--Best Variables. Regression runs for the 17th and 18th of March (N = 180) indicated very little correlation between the independent variables (satellite parameters) and the dependent variable of "sea level pressure" (SLP). Thus, the predictand of SLP was dropped from further investigations.

The dependent variable of "weather and obstructions to vision" (PRE) was encoded according to Table 2.4-1. Although the coding system

used forces this predictand to be continuous (but non-linear) the predictand did correlate to the extent that typical derived regression equations yielded an $R^2$ of 0.30 to 0.35 by using four ATS variables as predictors. These results were consistently achieved for N's of 100-800. Due to the abnormal characteristics of encoding PRE and the lack of a more meaningful $R^2$, this predictand was considered unworthy of further investigation in its encoded form.

However, an attempt at improving the regression results of PRE was made by essentially recoding "weather and obstructions to vision" into a four-valued step function called CIP as shown in Table 2.4-1. The resulting regression equations for the predictand CIP yielded $R^2$ values between 0.25 and 0.35 for similar case conditions used for deriving the PRE regression equations. Thus, the predictand of CIP was also dropped from further investigation.

Visibility (VSBY) correlated best with the dependent variable of PRE as one would expect, but this relationship was not a primary objective of the study. Using 830 cases, three ATS predictors gave an $R^2$ of 0.25 with a standard error of 4.1 statute miles. Computer runs with less of a sample size indicated a maximum of 40% explained variation. However, since visibility is a significant operational weather parameter commonly used in terminal forecasting, the decision was made to retain this predictand for further experimentation in spite of the relatively low $R^2$ values achieved.

Total cloud amount (TCA) and total opaque cloud amount (TOCA) both correlated well with several ATS predictors; these were positive results of experiment 1. The predictand of TOCA consistently indicated

the highest $R^2$ values of all the dependent variables tested. Explained variations for the TOCA regressions ranged between 0.60 and 0.85 with the higher values occurring for small sample sizes of N = 90. Regressions for the predictand of TCA yielded smaller $R^2$ values by an average deviation of 0.10, relative to the explained variations for the TOCA regressions. In addition, the "opaque" standard error of estimate was consistently smaller. Thus, the opaque cloud amount was chosen for further investigation due to its apparent linear relationship with brightness.

The dependent variable of ceiling (CLG) correlated best with the parameter of total opaque cloud amount. Regressions of CLG on the ATS brightness statistics yielded $R^2$'s as high as 0.85 for small sample sizes of 50-100. Using an N of 741 which included several days of mostly clear skies, three ATS predictors accounted for 58% of the total variation of ceiling, albeit the computed standard error was near 10,000 feet. These results were considered meaningful since the regression equations accounted for most of the variation of a useful weather parameter over an encoded range of 40,000 feet.

Among all the satellite independent variables tested, the highest correlations were obtained form the mean grid brightness ($\overline{B}_i$). The standard deviation of the mean grid brightness ($SD_i$) which is indicative of brightness dispersion was also an important satellite predictor. The remaining satellite independent variables contributed in a manner which needs further study regarding physical interpretation . The upper air and a prior independent variables were used in subsequent experiments and their contributions will be noted in these experimental results.

The conclusion of experiment 1 was that total opaque cloud amount, visibility, and ceiling were significantly correlated with the ATS brightness parameters to the extent that further experiments would center on improving these derived relationships.

Experiment 2 -- Grid Size. The two grid sizes were contrasted in seven different runs using N's of 120-165. For the 0 and 2 hour lag trials, the smaller grid of $0.5^{o}$ x $0.5^{o}$ yielded better statistical results by explaining an average of 3.6% more of total variation. For example, using two days of relatively little cloudiness, the 50 nm grid yielded an $R^2$ of 0.36 for CLG while the same data with the 25 nm grid yielded 0.39. The predictands used during this experiment were CLG and TOCA. Regressions for a 4 hour lag time indicated that the experimental grid was too small to account for the necessary advection since the mean radius of coverage around each terminal was only 40 nm.

The conclusion from this experiment was that the 25 nm grid distance was more beneficial, both economically and statistically, for special cases with little or no advection. However, for the spectrum of cases to be investigated by later experiments, the 50 nm grid distance was required for the longer lag times.

Experiment 3 -- General Equations and Lag Times. This was the first of the primary experiments of the project. For experiment 3, and all the remaining experiments, the ATS data from the 50 nm grid were used as predictors with CLG, VSBY and TOCA as predictands.

Using N = 635 , general regression equations were derived for all terminals and all data times, with lags of 0, 2, 4 and 6 hours. These general MRE's are shown in Table 4.1-1 along with the respective $R^2$

and S for each equation. Abbreviations for all variables used in the equations are given in Table 3.2-1. All equations are written in decreasing order of predictor significance with two, three, or four ATS independent variables included. The addition of further predictors typically increased $R^2$ by less than 1% due to the high interdependence of the ATS variables. Equations derived for the shorter lag times exemplify the physical relationship between the predictands and the reflected radiance measurements at the central grid, number 5. Regression equations for the 4 and 6 hour lag times reveal a preference for grid number 3, which is indicative of mean advection from a southwesterly direction.

Considering the total independence of the satellite observations from any conventional meteorological data, as well as the current state of statistical weather prediction on these short time scales, we judge the data of Table 4.1-1 as very encouraging initial results. For comparison, Glahn and Allen (1971) report percent reduction of variance ($100*R^2$) of terminal ceiling and visibility of 20-30% and 15-22%, respectively from 3-6 hour statistical forecasts. Their predictors were chosen from surface weather observations at a network of stations near each predictand terminal. Predictions of probability of precipitation (POP) by Klein (1971) over a wide range of U. S. stations (as we did) and over all seasons yielded a mean reduction of variance of 40% and a standard error equal to 30% of his variable range. In this case, his predictors included 850 mb height and previous 12 hour precipitation measured at the terminal.

A graphical depiction of the general regression equation results is shown in Figure 4.1.1. Here, $R^2$ values are displayed against lag time. Except for visibility, a small decrease in reduction of variance

TABLE 4.1-1

DERIVED GENERAL REGRESSION EQUATIONS - ATS VARIABLES ONLY

| | | |
|---|---|---|
| 0 hr lag<br>N = 635 | $\hat{CLG}$ = | 441.54 - 2.54 (MN5) + 1.00 (DMD-7) - 2.20 (SD-6)<br>$R^2$ = 0.66 S = 9575. |
| 0 hr lag<br>N = 635 | $\hat{VSBY}$ = | 12.98 - 0.06 (MN6) + 0.13 (SD-4) + 0.03 (DMT-6)<br>$R^2$ = 0.31 S = 4.08. |
| 0 hr lag<br>N = 635 | $\hat{TOCA}$ = | -0.88 + 0.07 (MN5) + 0.09 (SD-5) + 0.03 (DMD-6)<br>$R^2$ = 0.69 S = 2.32. |
| 2 hr lag<br>N = 635 | $\hat{CLG}$ = | 434.17 - 2.46 (MN5) + 1.31 (DMD-7) - 1.96 (SD-7)<br>$R^2$ = 0.61 S = 9995. |
| 2 hr lag<br>N = 635 | $\hat{VSBY}$ = | 13.55 - 0.06 (MN6) + 0.12 (SD-4) + 0.04 (DMT-6)<br>$R^2$ = 0.34 S = 3.95. |
| 2 hr lag<br>N = 635 | $\hat{TOCA}$ = | -0.46 + 0.06 (MN5) + 0.07 (SD-2) - 0.03 (DMD-7)<br>$R^2$ = 0.65 S = 2.45. |
| 4 hr lag<br>N = 635 | $\hat{CLG}$ = | 418.01 - 1.23 (MN5) - 0.92 (MN3) - 0.49 (MN9)<br>$R^2$ = 0.56 S = 10376. |
| 4 hr lag<br>N = 635 | $\hat{VSBY}$ = | 14.02 - 0.05 (MN6) + 0.14 (SD-4) - 0.02 (MN2)<br>$R^2$ = 0.39 S = 3.80. |
| 4 hr lag<br>N = 635 | $\hat{TOCA}$ = | 0.03 + 0.03 (MN5) + 0.03 (MN3) + 0.06 (SD-3)<br>$R^2$ = 0.55 S = 2.67. |
| 6 hr lag<br>N = 635 | $\hat{CLG}$ = | 414.64 - 2.62 (MN3) + 2.28 (DMD-3) + 1.27 (DMD-7)<br>$R^2$ = 0.54 S = 10562. |
| 6 hr lag<br>N = 635 | $\hat{VSBY}$ = | 14.34 - 0.05 (MN6) + 0.13 (SD-4) - 0.02 (MN2)<br>$R^2$ = 0.39 S = 3.81 |
| 6 hr lag<br>N = 635 | $\hat{TOCA}$ = | 0.50 + 0.10 (MN3) - 0.09 (DMD-3) - 0.03 (MN7)<br>$R^2$ = 0.50 S = 2.87 |

occurs at longer lag times. The same figure shows the $R^2$ values that would result from a regression equation using a priori values[1] of the predictands as predictors. This essentially shows the results of a forecast based on persistence. Note that $R^2 = 1.00$ for the "persistence" forecast at 0 hour lag. In all cases, the results from persistence decrease rapidly with lag time and (except for visibility) reach or fall below the satellite-derived $R^2$ results at 3-6 hours.

Experiment 4 -- Upper Air Predictions. Inclusion of the five upper air parameters as predictors yielded insignificant $R^2$ increases for both the CLG and TOCA equations, as shown in Figure 4.1-1. This graph depicts the $R^2$ values obtained as a function of lag time and type of predictors used in the regression equation, and demonstrates that upper air predictors alone yield explained variations of 15-30%.

The conclusion of experiment 4 was that the addition of the upper air predictors were not significant for yielding more useful equations than those derived in experiment 3.

Experiment 5 -- Vorticity and Wind Stratification. Approximately 11% of the total data set qualified for the PVA and NVA categories which led to an experimental $N$ of 99 for this investigation. Table 4.1-2 is used to summarize the results of this experiment by showing only the new $R^2$ values that are higher than those obtained from the general equations of experiment 3.

---

[1] The a priori values used are defined as the values of the predictands at time $t = 0$ (the time of the ATS parameters).

Figure 4.1-1

CLG =

| | | |
|---|---|---|
| 1) | 441.54 - 2.54(MN5) + 1.00(DMD-7) - 2.20(SD-6) | S = 9575 ft. |
| 2) | 434.17 - 2.46(MN5) + 1.31(DMD-7) - 1.96(SD-7) | S = 9995 ft. |
| 3) | 418.01 - 1.23(MN5) - 0.92(MN3) - 0.49(MN9) | S = 10376 ft. |
| 4) | 414.64 - 2.62(MN3) + 2.28(DMD-3) + 1.27(DMD-7) | S = 10562 ft. |
| 5) | NONE | |
| 6) | 49.34 + 0.78(APICLG) | S = 9449 ft. |
| 7) | 72.76 + 0.67(APICLG) | S = 11033 ft. |
| 8) | 78.38 + 0.64(APICLG) | S = 11503 ft. |
| 9) | 441.54 - 2.54(MN5) + 1.00(DMD-7) - 2.20(SD-6) | S = 9575 ft. |
| 10) | -800.05 - 2.26(MN5) + 2.11(AVGZ) - 1.33(AVGC) | S = 9693 ft. |
| 11) | -463.84 - 1.43(MN5) - 1.08(MN3) + 1.56(AVGC) | S = 10199 ft. |
| 12) | 414.64 - 2.62(MN3) + 2.28(DMD-3) + 1.27(DMD-7) | S = 10562 ft. |
| 13) | -889.48 - 3.51(AVGV) + 1.93(AVGZ) | S = 14701 ft. |
| 14) | 1512.76 - 3.80(AVGV) + 3.04(AVGZ) | S = 13641 ft. |
| 15) | -1341.12 - 3.44(AVGV) + 2.74(AVGZ) | S = 13706 ft. |
| 16) | 291.16 - 3.49(AVGV) + 4.74(AVGT) | S = 14013 ft. |

VSBY =

| | | |
|---|---|---|
| 1) | 12-98 - 0.06(MN6) + 0.13(SD-4) + 0.03(DMT-6) | S = 4.08 |
| 2) | 13.55 - 0.06(MN6) + 0.12(SD-4) + 0.04(DMT-6) | S = 3.95 |
| 3) | 14.02 - 0.05(MN6) + 0.14(SD-4) - 0.02(MN2) | S = 3.80 |
| 4) | 14.34 - 0.05(MN6) + 0.13(SD-4) - 0.02(MN2) | S = 3.81 |
| 5) | NONE | |
| 6) | 1.27 + 0.90(APVSBY) | S = 1.99 |
| 7) | 2.27 + 0.82(APVSBY) | S = 2.68 |
| 8) | 2.97 + 0.76(APVSBY) | S = 3.12 |
| 9) | 53.09 - 0.06(MN6) - 0.07(AVGZ) + 0.11(SD-4) + 0.04(AVGU) | S = 3.88 |
| 10) | 9.27 - 0.06 (MN6) - 0.15(AVGT) + 0.11(SD-4) + 0.05(AVGU) | S = 3.77 |
| 11) | 11.20 - 0.07(MN6) + 0.13(SD-4) - 0.13(AVGT) | S = 3.74 |
| 12) | 11.91 - 0.05(MN6) + 0.13(SD-4) - 0.12(AVGT) - 0.02(MN2) | S = 3.72 |
| 13) | 5.46 - 0.08(AVGV) + 0.06(AVGU) - 0.12(AVGT) | S = 4.50 |
| 14) | 6.53 - 0.09(AVGV) + 0.06(AVGU) - 0.08(AVGT) | S = 4.48 |
| 15) | 8.75 - 0.10(AVGV) + 0.04(AVGU) | S = 4.48 |
| 16) | 9.16 - 0.10(AVGV) + 0.03(AVGU) | S = 4.48 |

TOCA =

| | | |
|---|---|---|
| 1) | -0.88 + 0.07(MN5) + 0.09(SD-5) + 0.03(DMD-6) | S = 2.32 |
| 2) | -0.46 + 0.06(MN5) + 0.07(SD-2) - 0.03(DMD-7) | S = 2.45 |
| 3) | 0.03 + 0.03(MN5) + 0.06(SD-3) + 0.03(MN3) | S = 2.67 |
| 4) | 0.50 + 0.10(MN3) - 0.09(DMD-3) - 0.03(MN7) | S = 2.87 |
| 5) | NONE | |
| 6) | 0.75 + 0.86(APTOCA) | S = 2.02 |
| 7) | 1.44 + 0.75 (APTOCA) | S = 2.48 |
| 8) | 1.78 + 0.69(APTOCA) | S = 2.86 |
| 9) | -0.88 + 0.07(MN5) + 0.09(SD-5) + 0.03(DMD-6) | S = 2.32 |
| 10) | 29.21 + 0.06(MN5) - 0.05(AUGZ) + 0.04(AVGV) | S = 2.42 |
| 11) | 32.26 + 0.05(MN5) - 0.05(AVGZ) + 0.04(AVGV) | S = 2.61 |
| 12) | 0.50 + 0.10(MN3) - 0.09(DMD-3) - 0.03(MN7) | S = 2.87 |
| 13) | 36.57 + 0.10(AVGV) - 0.05(AVGZ) | S = 3.68 |
| 14) | 47.95 + 0.10(AVGV) - 0.07(AVGZ) | S = 3.49 |
| 15) | 73.74 + 0.10(AVGV) - 0.12(AVGZ) - 0.26(AUGVOR) | S = 3.37 |
| 16) | 69.04 + 0.09(AVGV) - 0.11(AUGZ) - 0.33(AUGVOR) | S = 3.52 |

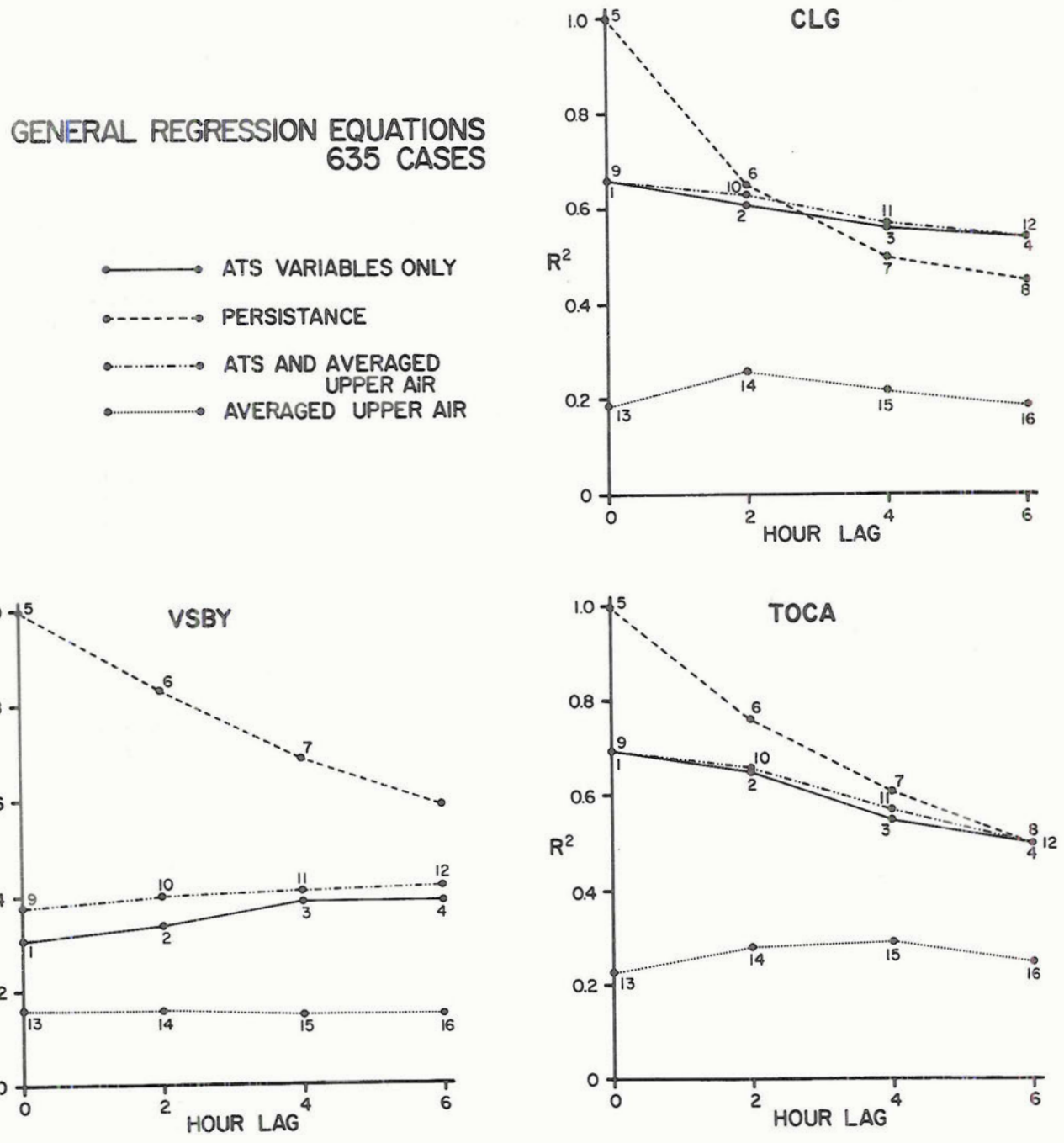


Figure 4.1-1. Graphical display of results of the general regression experiments; contrast with persistence.

CASES WHERE $R^2$ FOR STRATIFIED CASE EXCEEDED THE GENERAL CASE

| STRATIFICATION CRITERIA | 0 HR LAG | | | 2 HR LAG | | | 4 HR LAG | | | 6 HR LAG | | |
|---|---|---|---|---|---|---|---|---|---|---|---|---|
| | $R^2$ CLG | $R^2$ VSBY | $R^2$ TOCA | $R^2$ CLG | $R^2$ VSBY | $R^2$ TOCA | $R^2$ CLG | $R^2$ VSBY | $R^2$ TOCA | $R^2$ CLG | $R^2$ VSBY | $R^2$ TOCA |
| PVA | --- | --- | --- | .66 | --- | .68 | .63 | .40 | --- | .61 | .42 | .57 |
| OVA | .75 | .48 | .73 | .71 | .58 | .73 | .63 | .64 | .68 | .68 | .63 | .64 |
| NVA | .67 | --- | .80 | --- | .35 | --- | --- | --- | .60 | --- | .47 | --- |
| 500 mb winds $301^{o}$-$360^{o} \leq$ 40 KTS | --- | --- | .71 | --- | --- | .74 | --- | --- | --- | --- | --- | .52 |
| 500 mb winds $240^{o}$-$300^{o} \leq$ 30 KTS | .71 | .42 | .74 | .72 | .37 | .72 | .62 | .40 | .61 | .61 | .40 | .56 |



EXPERIMENT 5

VORTICITY AND WIND STRATIFICATION

Table 4.1-2

The category of OVA yielded consistently better results for all lags and each of the three predictands. The categories of PVA and NVA showed sporadic improvements for various lags and predictands.

Regression equations derived under the stratification for west wind direction and moderate speeds indicate higher $R^2$ values for all lag times and all predictands, although a similar stratification for northwesterly advection shows $R^2$ increases only in the 0, 2 and 6 hr. equations for TOCA.

Experiment 6 -- Geographic Stratification. Using all the applicable cases over the 12 data days, regression equations were derived for various terminal combinations. For example, equations for only Los Angeles (LAX) and San Francisco (SFO) revealed a large reduction of $R^2$ for CLG and TOCA, but this was attributed to a general lack of cloudiness since only one data day experienced predominant clouds below 20,000 feet. However, the equations for predicting VSBY for all terminals except the midwest (LBF, OMA, SGF, and TUL) were of more usefulness with $R^2$ values often exceeding 50% (Table 4.1-3). For those midwest stations, the regional stratification raised the explained variance of ceiling and opaque cloud amount to values of 0.6 - 0.71 (correlation coefficients of 0.75 - 0.85).

Figures 4.1-2 and 4.1-3 show the variation of $R^2$ with lag time for the Midwest and Northeast regions. In the latter, the spring time terminal weather would be very difficult to forecast by persistence and the geosynchronous satellite data predictors continue to show better results for CLG and TOCA.

Experiment 6 showed that terminal stratification definitely aids visibility forecasts over all time periods at most locations.

CASES WHERE $R^2$ FOR STRATIFIED CASE EXCEEDED THE GENERAL CASE

| TERMINALS | 0 HR. LAG | | | 2 HR. LAG | | | 4 HR. LAG | | |
|---|---|---|---|---|---|---|---|---|---|
| | $R^2$ CLG | $R^2$ VSBY | $R^2$ TOCA | $R^2$ CLG | $R^2$ VSBY | $R^2$ TOCA | $R^2$ CLG | $R^2$ VSBY | $R^2$ TOCA |
| LBF, OMA SGF, TUL | .69 | ---- | .71 | .65 | ---- | .71 | .60 | ---- | .61 |
| LAX, SFD | ---- | .50 | ---- | ---- | .45 | ---- | ---- | .49 | ---- |
| ALB, DCA, LGA | ---- | .40 | ---- | ---- | .45 | ---- | ---- | .50 | ---- |
| SLC, DEN | ---- | .56 | ---- | ---- | .49 | .67 | .61 | .57 | .58 |
| ORD | ---- | .51 | ---- | ---- | .65 | ---- | ---- | .57 | ---- |

EXPERIMENT 6

TERMINAL STRATIFICATION

Table 4.1-3

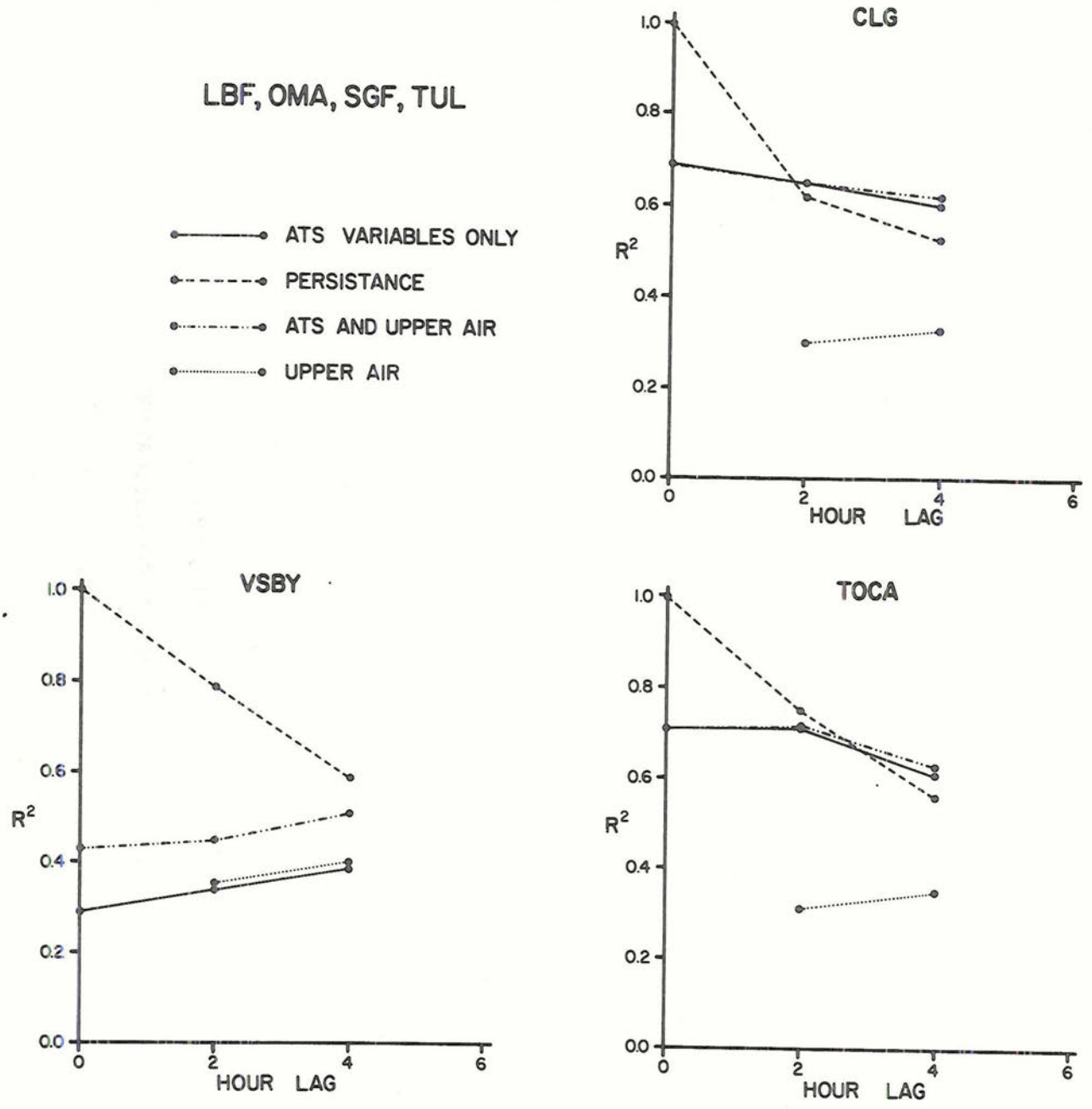


Figure 4.1-2. Graphical display of results of regression experiments over midwest United States.

Figure 4.1-3

CLG =

| | | |
|---|---|---|
| 1) | 390.50 - 2.10(MN8) - 3.28(SD-8) | S = 9822 ft. |
| 2) | 419.31 - 2.28(MN5) - 3.85(SD-5) + 2.20(DMD-5) | S = 10209 ft. |
| 3) | 346.14 - 1.84(MN6) - 4.41(SD-7) + 2.86(SD-9) | S = 10578 ft. |
| 4) | NONE | |
| 5) | 70.90 + 0.56(APICLG) | S = 11257 ft. |
| 6) | 100.56 + 0.42(APICLG) | S = 11956 ft. |
| 7) | 450.25 - 2.05(MN8) - 3.35(SD-8) - 6.31(AVGVOR) | S = 9654 ft. |
| 8) | 449.37 - 1.71(MN5) - 13.18(AVGVOR) - 3.21(AVGV) | S = 9562 ft. |
| 9) | 369.87 - 1.99(MN6) - 4.30(SD-7) + 2.54(SD-9) + 1.28(DMD-8) | S = 10398 ft. |
| 10) | 375.34 - 43.97(AVGVOR) - 4.14(AVGV) - 12.40(AVGT) | S = 11879 ft. |
| 11) | 385.02 - 5.08(AVGV) - 36.57(AVGVOR) - 7.88(AVGT) | S = 11208 ft. |
| 12) | 188.26 - 2.77(AVGV) | S = 12777 ft. |

VSBY =

| | | |
|---|---|---|
| 1) | 14.54 - 0.04(MN9) - 0.06(DMD-5) + 0.05(DMD-7) | S = 3.29 |
| 2) | 14.59 - 0.06(MN9) + 0.10(SD-9) - 0.06(DMD-5) | S = 3.10 |
| 3) | 14.32 - 0.06(MN9) + 0.11(SD-9) + 0.05(DMD-7) | S = 3.04 |
| 4) | NONE | |
| 5) | 1.50 + 0.90(APVSBY) | S = 1.71 |
| 6) | 2.50 + 0.82(APVSBY) | S = 2.50 |
| 7) | 146.00 - 0.04(MN9) - 0.22(AVGZ) - 0.97(AVGVOR) | S = 2.84 |
| 8) | 14.59 - 0.06(MN9) + 0.10(SD-9) - 0.06(DMD-5) | S = 3.10 |
| 9) | 14.32 - 0.06(MN9) + 0.11(SD-9) + 0.05(DMD-7) | S = 3.04 |
| 10) | 147.24 - 0.22(AVGZ) - 1.05(AVGVOR) | S = 3.68 |
| 11) | 127.96 - 0.19(AVGZ) - 0.97(AVGVOR) | S = 3.82 |
| 12) | correlation insufficient for computation | |

TOCA =

| | | |
|---|---|---|
| 1) | 0.18 + 0.06(MN6) + 0.09(SD-8) | S = 2.12 |
| 2) | 0.06 + 0.06(MN6) + 0.09(SD-5) + 0.03(DMD-4) | S = 2.14 |
| 3) | 2.60 + 0.04(MN3) | S = 2.55 |
| 4) | NONE | |
| 5) | 1.66 + 0.76(APTOCA) | S = 2.00 |
| 6) | 3.20 + 0.53(APTOCA) | S = 2.53 |
| 7) | -2.12 + 0.06(MN6) + 0.09(SD-8) + 0.24(AVGVOR) | S = 1.99 |
| 8) | 23.80 + 0.05(MN6) + 0.11(SD-5) - 0.04(AVGZ) | S = 2.06 |
| 9) | 2.60 + 0.04(MN3) | S = 2.55 |
| 10) | 1.08 + 1.01(AVGVOR) + 0.09(AVGV) + 0.27(AVGT) | S = 3.08 |
| 11) | 2.28 + 0.10(AVGV) + 0.35(AVGVOR) | S = 2.99 |
| 12) | 6.04 + 0.05(AVGV) | S = 3.05 |

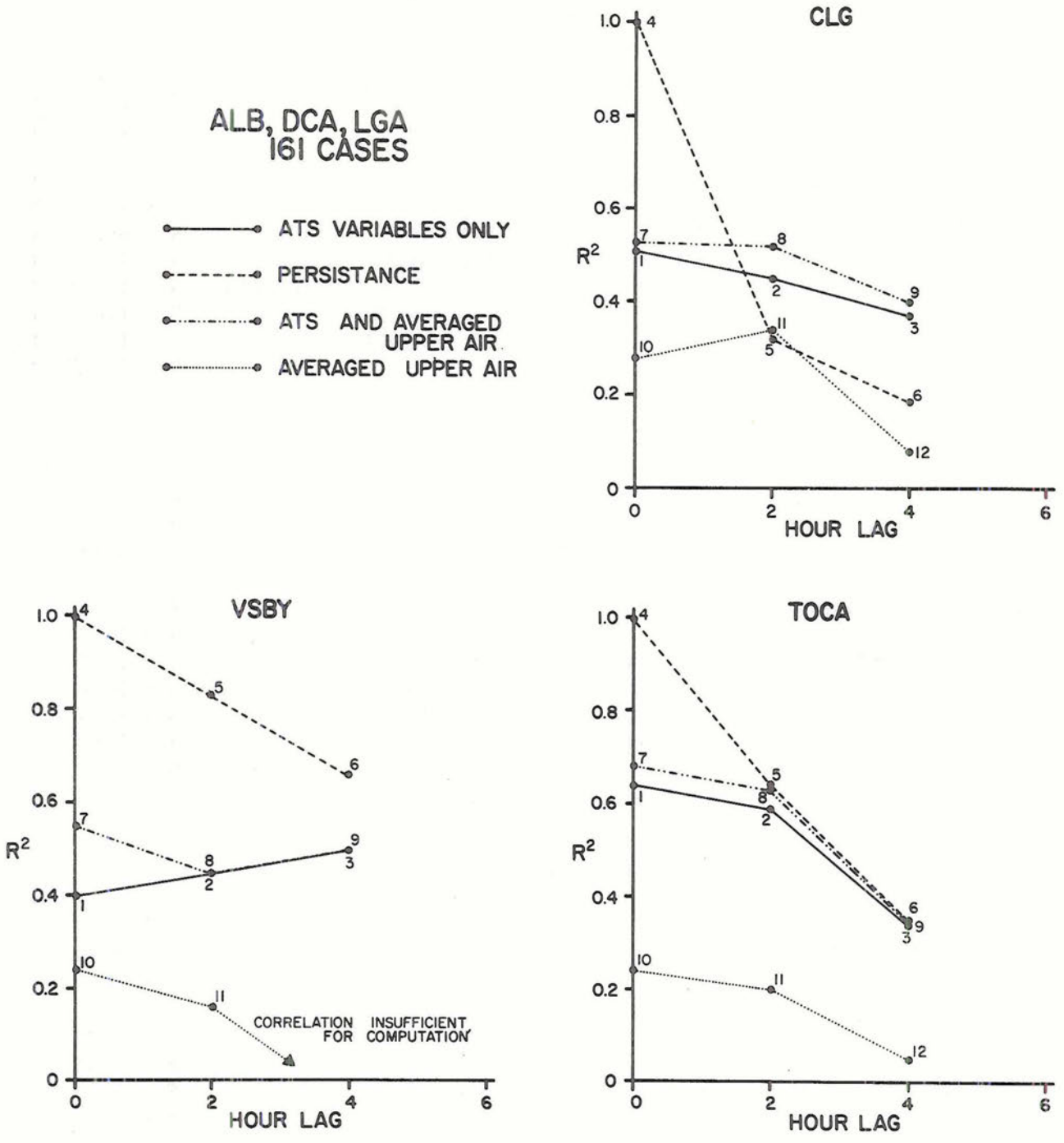


Figure 4.1-3. Graphical display of results of regression experiments over northeast United States terminals; contrast with persistence.

Experiment 7 -- Stratification for Cloud Cases. This experiment, outside the general goals of the present study, was a special attempt to objectively forecast terminal weather during complex weather situations. The experiment used 403 data cases selected from all available terminals having appropriate cloud conditions (see p. 35). All combinations of satellite parameters, upper air data and a priori values of the predictands themselves were screened in order to derive the best regression equations for these disturbed weather conditions. A side result showed that use of a priori observations of terminal visibility alone could explain more than 70% of the variance at 2 and 4 hour lags with standard errors of 2.4 - 3.0 miles. The satellite data alone provided better estimates of ceiling and opaque cloud cover than a priori values of these parameters (alone or in combinations). Although the standard errors from the satellite method were 10 to 11 thousand feet and 2 to 2.5 tenths of sky cover, they provide better objective forecasts under these rapidly changing conditions than does persistence.

## 4.2 Other Results

During the course of this project, a variable named PRE and alternately one termed CIP had been tested for regression development along with the prime variables of CLG, VSBY and TOCA. PRE was an attempt to span the reported values of weather and obstructions to vision with a continuous variable, CIP a similar attempt over only the more severe weather categories. Results of all regression runs for these variables were poor, most probably a result of the artificial adoption of the continuous variable approach. Additional efforts to predict short-term

variations of weather by class or by the probability of significant weather using geosynchronous satellite observations should be more successful.

As noted in Table 2.4-1, in the absence of a reported cloud ceiling (due to lack of at least broken cloud conditions) we assigned values of a very high ceiling to the data cases. This was done with the knowledge that a bimodal sample would result, but the prospect of stratification of the data sets and the need to retain a large number of cases covering all weather conditions caused the high-level ceiling assignment to be retained. This approach has effected all results of ceiling prediction quoted thus far and to assess the absolute value of this effect a special test was devised.

Using only 51 data cases from DEN and SLC where actual ceilings were reported, regression equations were developed in the normal manner. At 2 and 4 hour lags (a 6 hour lag was not attempted) the reduction of ceiling variance ($R^2$) was 0.70 with standard errors of about 5000 feet. This represents an absolute improvement in variance reduction of 10% and a 4000 ft. improvement in standard error over the DEN and SLC sample when ceiling values were arbitrarily extended over a wider range. Thus, errors in ceiling forecasts reported throughout this study must be considered worst case estimates wherein the satellite data predictors have been forced to operate without guidance or bias over a bimodal distribution of ceiling values. It appears that the ceiling errors could be cut 50% by development of special regression equations, still using only satellite data as predictors, but chosen for development and use only over areas of broken or overcast clouds. Another possible approach might be the use of a REEP (regression estimation of event probability) which attempts to forecast (using satellite data) the probability of occurrence of specific categories of low level ceilings.

## 5.0 Tests for Forecasting Significance and Usefulness

As noted in section 3.3, an independent, randomly selected data set was withheld from all regression equation development experiments. This set of 81 data cases was used to test all general regression equations derived from the N = 635 sample (Table 4.1-1). Such tests allow a measure of the stability of the derived equations and thus permit a more conclusive estimate of forecasting significance and usefulness. A sample of this intercomparison is:

| PARAMETER AND LAG | DEVELOPMENT SET | | INDEPENDENT SET | | |
|---|---|---|---|---|---|
| | $R^2$ | S | RE | SEE | REP |
| CLG ( 0 HR LAG) | 0.66 | 9575 | 0.51 | 10851 | N.A. |
| CLG ( 4 HR LAG) | 0.56 | 10376 | .45 | 10484 | -0.20 |
| VSBY (2 HR LAG) | 0.34 | 3.95 | 0.17 | 4.32 | 0.79 |
| VSBY (6 HR LAG) | 0.39 | 3.81 | 0.24 | 0.24 | 0.69 |
| TOCA (0 HR LAG) | 0.69 | 2.32 | 0.58 | 2.48 | N.A. |
| TOCA (6 HR LAG) | 0.50 | 2.87 | 0.43 | 2.86 | 0.20 |

For the independent set the parameter chosen for compairons with reduction of variance ($R^2$) and standard error (S) are the reduction of error:

$$RE = \left[ 1.0 - \frac{\Sigma(Y^0 - Y^F)^2}{\Sigma(Y^0 - \bar{Y}^0)^2} \right] \qquad (3)$$

where $Y^0$ is observed value, $Y^F$ the forecast value, $\bar{Y}^0$ is mean of $Y^0$ and the standard error of estimate:

$$SEE = \left[ \frac{\Sigma(Y^0 - Y^F)^2}{N} \right]^{\frac{1}{2}} \qquad (4)$$

Additional comparison of our results with those which would have been derived using a multiple regression approach based on persistence are shown by the REP[1] column. This percent reduction of error in the independent set by persistence forecasting is less than our satellite-parameter method except when the predictand is visibility.

Results from the independent sample test indicate good stability of our derived regression equations within the general uncertainty limit of this new approach. Furthermore, the checks have again noted, as in section 4, that the ATS satellite predictors out-perform persistence forecasting in the 3-6 hour range for the variables of air terminal cloud ceiling and amount of total opaque cloud cover.

With our independent test set of 81 data cases, we have also derived the absolute values of the RMS deviations of the forecast from the observed parameters for:

a) the satellite parameter method:

$$RMS_S = SEE = \left[\frac{\Sigma(Y^0 - Y^F)^2}{N}\right]^{\frac{1}{2}}$$

b) a method using persistence (a priori variables as predictors):

$$RMS_P = \left[\frac{\Sigma(Y^0 - Y^{AP})^2}{N}\right]^{\frac{1}{2}} \qquad (6)$$

c) and the deviation that would be found from a method that would always forecast the climatological value:

$$MAD = \frac{\Sigma|Y^0 - \bar{Y}^0|}{N} \qquad (7)$$

---

[1] REP is derived from a form of Eq. 1 with $Y^{AP}$, an a priori variable, substituted for $Y^F$.

These results are shown in Figure 5.0-1. The RMS variation of the 81 test samples used is noted by an X in the figure. The RMS deviation or error is inversely related to the reduction of variance discussed in the development set. For the persistence case it rises rapidly with time lag and exceeds the error from the satellite technique at 2 hours for ceiling, 2 hours for TOCA and not at all for visibility. The curve used to represent the skill of a climatology-based forecast (MAD) yields a worse error than the satellite method for ceiling and opaque cloudiness and no better results at any lag time for visibility.

There are a great variety of skill scores in use to assess the usefulness or success of forecasting methods. Many of them, derived to evaluate predictions expressed as the probability of an event occurring in a given class, are not appropriate to this study. Others require that climatological data be used to define class intervals in a contingency table (Ponofsky and Brier, 1965). Although this approach is feasible, it is beyond the scope of the present study. Thus, to test the results of our forecasts which are expressed on a continuous numerical scale, the RMS method used is most appropriate.

## 6.0 Conclusions and Recommendations

This study has demonstrated that short-term statistical forecasts of ceiling and total opaque cloud amount can be made with the use of only ATS III geosynchronous satellite data. The linear, least squares,

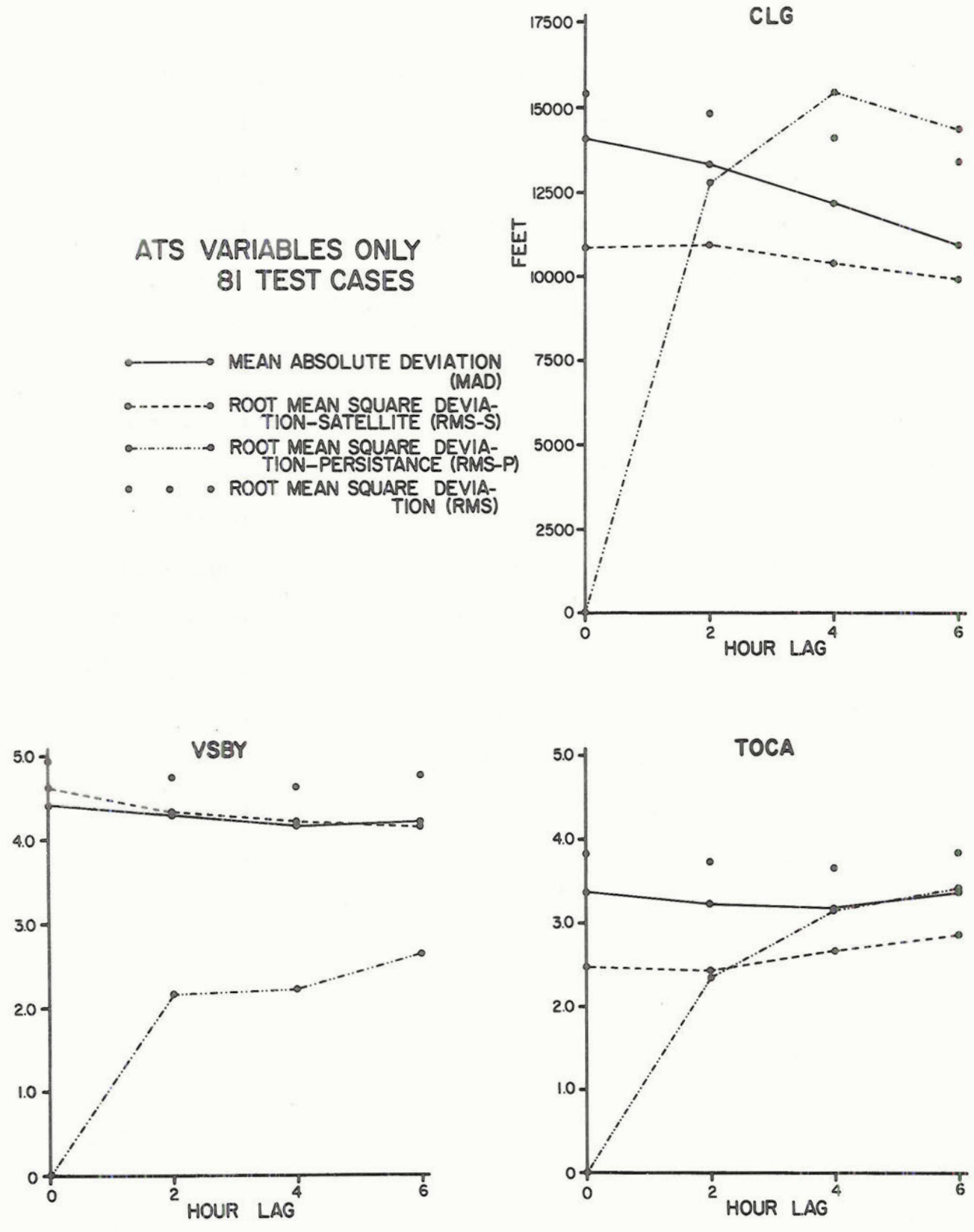


Figure 5.0-1. RMS error of statistical forecasts using satellite data compared to forecast error in results based on climatology (MAD) and on persistence ($RMS_p$)

multiple regression equations explain 50 - 70% of the predictands' total variation for forecast periods of up to six hours. As a general comparison, the NMC adopted regression equations for predicting maximum and minimum surface temperatures for 12-60 hour projections explain an average of 75% of the temperature variance (Klein and Lewis, 1970). However, other techniques under development to produce terminal forecasts and probability of precipitation forecasts presently explain only 30% of the predictand variance.

The operational utility of the results of the present study is limited for some applications due to the large standard errors which represent 20-25% of the predictands' range. However, substantial improvement in the prediction equations appears possible if appropriate stratification criteria are applied to the data set. Further research will be required to identify and refine these criteria to the extent of making the regression equations operationally significant. In the context of the present study, which uses satellite observations only, the stratification criterion should be a parameter readily observed or forecast from satellite data. Thus, the total technique would be independent of surface observations and would be applicable on a global basis and especially valuable over the oceanic regions.

The present study was established that geosynchronous meteorological data are a valuable new type of information for short-term statistical forecasts of mesoscale phenomena. The full potential of these data as stand-alone objective forecast predictors awaits future study. However, at the present time, results of this study show that 2-6 hour local area forecasts could be added by the objective "guidance" provided by geosynchronous satellite data used in multiple regression equations. A

field test is recommended. Furthermore, the present study was developed and tested using point-site (terminal) weather data for input and verification. Use of a local area approach (i.e., stratification by geography) may yield even better results than the general results of the present study.

It is important to note that the array of satellite data over a region allowed study of both advection and development of the cloud fields. In addition to mean variance values at grid points, the pattern of clouds at a grid mesh, as well as the relative large scale distribution and time rate of change of the cloud fields, were all parameters that weighted heavily into the prediction equations. Great care was necessary in processing the experimental ATS-3 satellite data so as to insure the ability for unbiased intra- and inter-daily measurement comparison. Future research with the geosynchronous satellite data as applied to very short range forecasting should include study of the new possibilities of using infrared radiance measurements.

multiple regression equations explain 50 - 70% of the predictands' total variation for forecast periods of up to six hours. As a general comparison, the NMC adopted regression equations for predicting maximum and minimum surface temperatures for 12-60 hour projections explain an average of 75% of the temperature variance (Klein and Lewis, 1970). However, other techniques under development to produce terminal forecasts and probability of precipitation forecasts presently explain only 30% of the predictand variance.

The operational utility of the results of the present study is limited for some applications due to the large standard errors which represent 20-25% of the predictands' range. However, substantial improvement in the prediction equations appears possible if appropriate stratification criteria are applied to the data set. Further research will be required to identify and refine these criteria to the extent of making the regression equations operationally significant. In the context of the present study, which uses satellite observations only, the stratification criterion should be a parameter readily observed or forecast from satellite data. Thus, the total technique would be independent of surface observations and would be applicable on a global basis and especially valuable over the oceanic regions.

The present study was established that geosynchronous meteorological data are a valuable new type of information for short-term statistical forecasts of mesoscale phenomena. The full potential of these data as stand-alone objective forecast predictors awaits future study. However, at the present time, results of this study show that 2-6 hour local area forecasts could be added by the objective "guidance" provided by geosynchronous satellite data used in multiple regression equations. A

field test is recommended. Furthermore, the present study was developed and tested using point-site (terminal) weather data for input and verification. Use of a local area approach (i.e., stratification by geography) may yield even better results than the general results of the present study.

It is important to note that the array of satellite data over a region allowed study of both advection and development of the cloud fields. In addition to mean variance values at grid points, the pattern of clouds at a grid mesh, as well as the relative large scale distribution and time rate of change of the cloud fields, were all parameters that weighted heavily into the prediction equations. Great care was necessary in processing the experimental ATS-3 satellite data so as to insure the ability for unbiased intra- and inter-daily measurement comparison. Future research with the geosynchronous satellite data as applied to very short range forecasting should include study of the new possibilities of using infrared radiance measurements.

## 7.0 References

Bartman, F. L., 1967: The reflectance and scattering of solar radiation by the earth. University of Michigan Technical Report, ORA Project No. 05863.

Brennan, B., and W. R. Bandeen, 1970: Anisotropic reflectance characteristics of natural earth surfaces. Journal of Applied Optics, Vol. 9, No. 2.

Committee on Atmospheric Sciences, 1971: The atmospheric sciences and man's needs; priorities for the future. National Academy of Sciences, Washington, D. C.

Dixon, W. J. (Ed.), 1970: Biomedical computer programs. University of California Publications in Automatic Computation, No. 2.

Draper, N. R., and H. Smith, 1966: Applied Regression Analysis. John Wiley and Sons, Inc., New York.

Glahn, H. and R. Allen, 1971: Preliminary results of a program for the automation of terminal forecasts, Proceedings of the 6th AWS Technical Exchange Conference, U. S. Naval Academy, 21 - 24 September, 1970.

Hadeen, K., 1971: Air Force Global Weather Central Boundary-Layer Model, Proceedings of the 6th AWS Technical Exchange Conference, U. S. Naval Academy, 21 - 24 September, 1970.

Keaty, J., and R. A. Allen, 1970: Development of base techniques for ceiling and visibility prediction. Report No. FAA-RD-70-22.

Klein, W., 1971: Computer prediction of precipitation probability in the United States, J. Appl. Meteor. , 10, 5, 903-915.

Klein, W. H., and F. Lewis, 1970: Computer forecasts of maximum and minimum temperatures. Journal of Applied Meteorology, Vol. 9.

Lorenz, E. N., 1969: Studies of atmospheric predictability. Report No. AFCRL-69-0119.

Panofsky, H. and G. Brier, 1965: Some Applications of Statistics to Meteorology, Pennsylvania State University, University Park, Pennsylvania.

Raschke, E., T. Vonder Haar, M. Pasternak, and W. Bandeen, 1971: Calculations of radiation balance of earth-atmospheric system form Nimbus III radiation measurements. NASA Technical Note (in press).

Stamm, A. J., and T. H. Vonder Haar, 1970: Atmospheric effects on remote sensing. University of Wisconsin, Space Science and Engineering Center, Final Project Report for Project No. 100823.

Suomi, V., and R. Parent, 1968: A color view of planet earth. Bulletin of the American Meteorological Society, Vol. 49, No. 2.

Suomi, V. E., and T. H. Vonder Haar, 1969: Geosynchronous meteorological satellite. Journal of Spacecraft and Rockets, Vol. 6, No. 3.

Vonder Haar, T. H., 1969: Meteorological applications of reflected radiance measurements from ATS-I and ATS-III. Journal of Geophysical Research, Vol. 74, No. 23.

Vonder Haar, T. H., and R. S. Cram, 1970: A pilot study on the application of geosynchronous meteorological satellite data to very short range terminal forecasting. Report No. AFCRL-70-0493.

Acknowledgements

We thank our colleagues Dr. Stephen Cox and Dr. Paul W. Mielke, Jr. for their suggestions, Mrs. Charlene Polifka for excellent computer programming and Mr. Jeff Gailiun for his assistance in many areas.

As project monitor, Mr. John Conover of Air Force Cambridge Research Laboratories aided this research with several contributions. The research was sponsored by the Electronic Systems Division of the U. S. Air Force Systems Command under Contract No. F19628-71-C-0073. The Colorado State University Computing Center provided a supplemental grant for computer time.

APPENDIX A.

Bi-directional Reflectance Models

If the ocean or a cloud were known to reflect solar radiation according to Lambert's Law (i.e., appeared as an isotropic reflector when viewed from different angles over a $2\pi$ steradian hemisphere by an instrument of fixed field of view), then the reflecting surface would always have the same "albedo" for any solar incident angle and any angle of view.

Since this is known to be not true, then the bi-directional reflectance ($\rho$, a property of the surface with units of steradians$^{-1}$) pattern of the surface must be taken into account. Using the following definitions:

$$\rho(\zeta,\theta,\psi) = \frac{\text{reflected radiation in the direction } \theta,\ \psi_2}{\text{incident radiation from a given } \zeta,\ \psi_1} =$$

$$= \text{bi-directional reflectance} \quad , \qquad \text{and}$$

$$r(\zeta) = \frac{\text{reflected radiation in all directions}}{\text{incident radiation from a given } \zeta,\ \psi_1} =$$

$$= \text{directional reflectance} \quad ,$$

where, according to Figure A-1:

$\zeta$ = solar zenith angle,

$\psi_1$ = solar azimuth angle,

$\theta$ = satellite zenith angle,

$\psi_2$ = satellite azimuth angle, and

$\psi = \psi_1 - \psi_2$ = relative solar azimuth angle.

The two reflectances are related through the equation

$$r(\zeta) = \int_0^{2\pi} \rho(\zeta,\theta,\psi)\cos\theta\ d\Omega =$$

$$= \int_0^{2\pi} \int_0^{\pi/2} \rho(\zeta,\theta,\psi)\cos\theta \sin\theta\ d\theta\ d\psi_2 \quad , \qquad \text{(A1)}$$

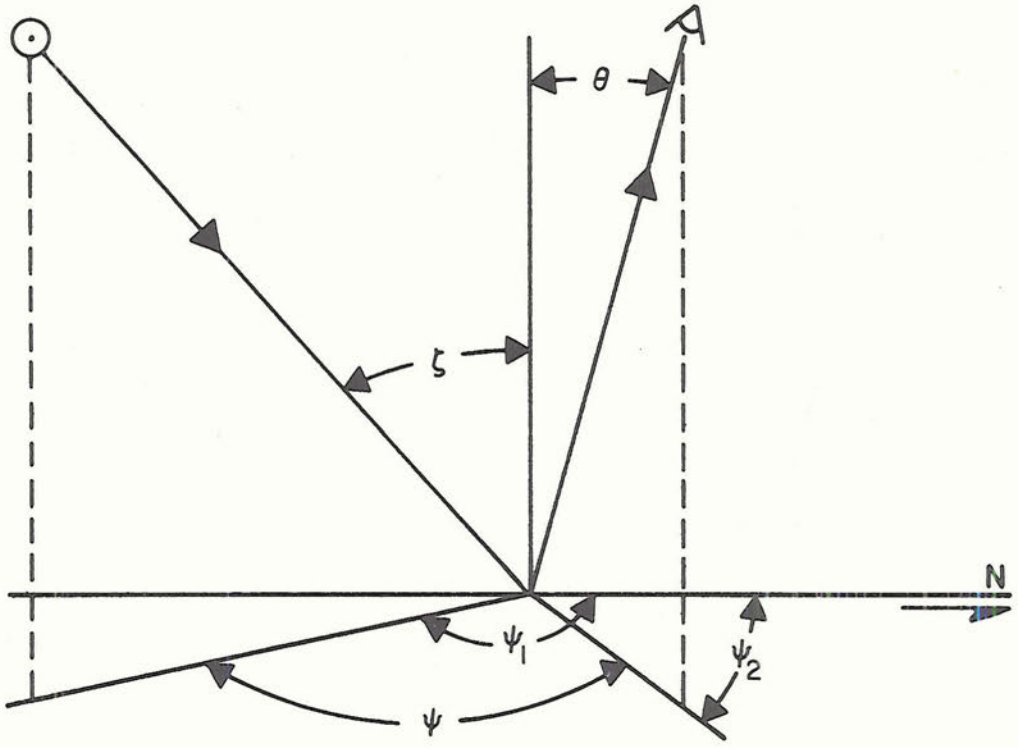


Figure A-1 Geometry of reflectance.

where $d\Omega$ represents the solid angle subtended by the sun at the reflecting surface. Since $\rho$ is independent of direction for a Lambertian surface, equation (1) reduces to

$$r = \pi\rho \quad . \tag{A2}$$

The isotropic reflectance from a Lambert surface (equation (2)) was then used as a common base from which the actual bi-directional reflectance $[\rho(\zeta,\theta,\psi)]$ was represented. Using observed cloud reflectivities of Brennan and Bandeen (1970) and others, as well as available summaries presented by Raschke et al. (1971), two models of bi-directional reflectance patterns were assembled. The first is an ocean bi-directional reflectance model; the second is a similar model for clouds. Anisotropic factors ($\chi$) were empirically found to represent the bi-directional reflectance of either a water surface or a cloud via the following equation.

$$\chi(\zeta,\theta,\psi) = \frac{r(\zeta)}{\pi\rho(\zeta,\theta,\psi)} \quad . \tag{A3}$$

Thus, $\chi < 1$ is indicative of reflected radiance greater than that which would be received from a Lambert surface when viewed under identical angular conditions $(\zeta,\theta,\psi)$, and vice versa for $\chi > 1$.

The angular dependence of ocean and cloud reflectance was accounted for via the $\chi$ factors as shown in Appendix B. In the case of clouds, other reflectance variables related to physical characteristics of the condensed water vapor are also important. Among these are the phase state and size distribution of the condensate, the amount of condensate and cloud thickness (Stamm and Vonder Haar, 1970). In addition, the nature of the underlying surface may affect the observed cloud reflectivities (Bartman, 1967). Direct inclusion of these other

variables is nearly impossible; however, the empirical $\chi$ observations do represent the integrated result of all relevant factors.

A vertical cross section through the three-dimensional, $\chi$ surface of the ocean model used is shown in Figure A-2. A similar cross section through the cloud model is seen in Figure A-3.

Anisotropic factors were formulated for the following ranges of the three critical angles:

1. Solar zenith ($\zeta$), a. $0° \leq \zeta < 35°$,
   b. $35° \leq \zeta < 60°$,
   c. $60° \leq \zeta < 80°$;
2. Satellite zenith ($\theta$), $0° \leq \theta \leq 60°$ for $\Delta\theta$ of $10°$;
3. Relative azimuth ($\psi$), $0° \leq \psi \leq 180°$ for $\Delta\psi$ of $30°$ (symmetry was assumed for $180° < \psi < 360°$).

The complete table values of $\chi(\zeta,\theta,\psi)$ which form a layered matrix of 3 x 6 x 6 are given in Tables A-1 and A-2.

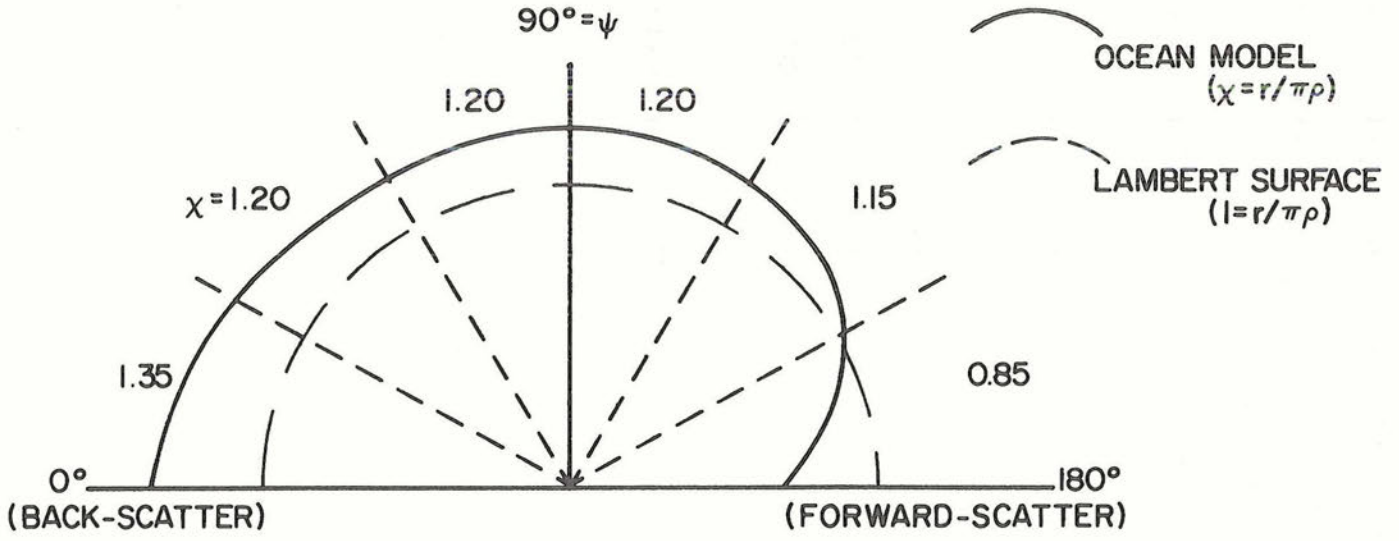


Figure A-2 Vertical cross-section through the χ model for the ocean depicting the difference in reflective characteristics between a Lambert surface and the observed ocean.
$\zeta$ = 35°-60°, $\theta$ = 20°-30°, $\psi$ = 0°-180°

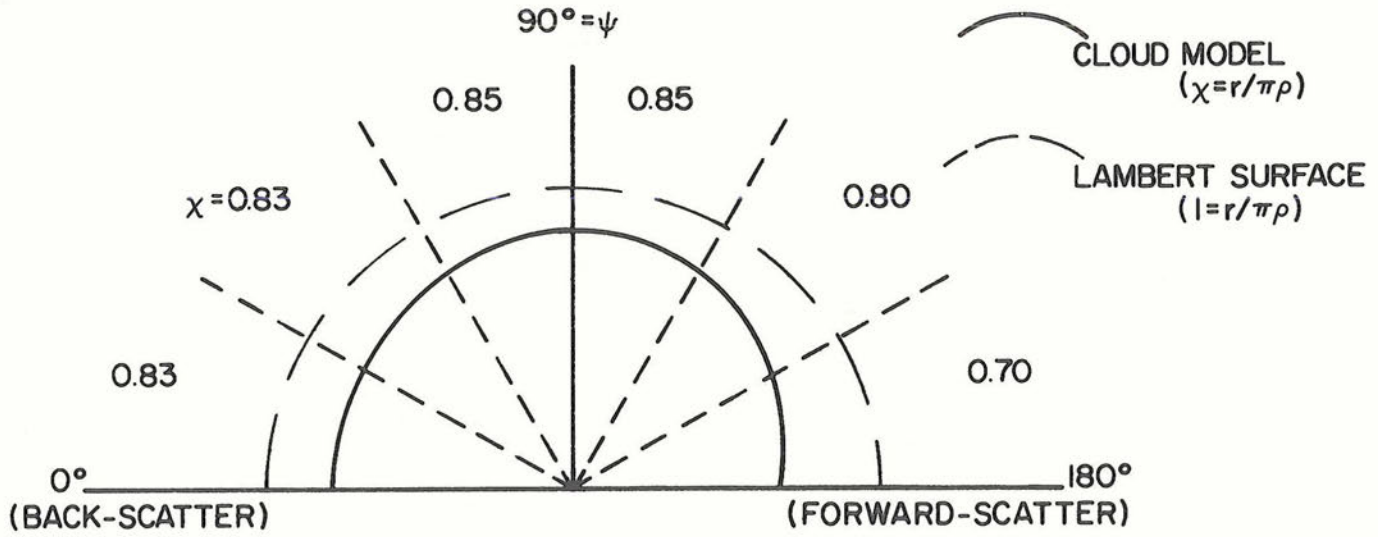


Figure A-3 Vertical cross-section through the χ model for a cloud depicting the difference in reflective characteristics between a Lambert surface and observed clouds.
$\zeta$ = 35°-60°, $\theta$ = 40°-50°, $\psi$ = 0°-180°

Table A-1

$\chi(\zeta,\theta,\psi)$ factors for the Nimbus III ocean model

1-A

$0° \leq \zeta < 35°$

| $\theta$ \ $\psi$ | 0°-30° | 30°-60° | 60°-90° | 90°-120° | 120°-150° | 150°-180° |
|---|---|---|---|---|---|---|
| 0°-10° | 1.40 | 1.40 | 1.40 | 1.30 | 1.20 | 1.20 |
| 10°-20° | 1.40 | 1.40 | 1.40 | 1.30 | 1.10 | 0.80 |
| 20°-30° | 1.40 | 1.40 | 1.40 | 1.25 | 0.90 | 0.50 |
| 30°-40° | 1.40 | 1.40 | 1.40 | 1.35 | 0.90 | 0.50 |
| 40°-50° | 1.20 | 1.20 | 1.25 | 1.25 | 1.05 | 0.70 |
| 50°-60° | 0.95 | 1.08 | 1.12 | 1.13 | 1.00 | 0.60 |

1-B

$35° \leq \zeta < 60°$

| $\theta$ \ $\psi$ | 0°-30° | 30°-60° | 60°-90° | 90°-120° | 120°-150° | 150°-180° |
|---|---|---|---|---|---|---|
| 0°-10° | 1.30 | 1.25 | 1.25 | 1.20 | 1.20 | 1.20 |
| 10°-20° | 1.35 | 1.25 | 1.20 | 1.20 | 1.20 | 1.05 |
| 20°-30° | 1.35 | 1.20 | 1.20 | 1.20 | 1.15 | 0.85 |
| 30°-40° | 1.25 | 1.10 | 1.10 | 1.15 | 0.98 | 0.55 |
| 40°-50° | 1.10 | 1.05 | 1.08 | 1.15 | 0.95 | 0.35 |
| 50°-60° | 1.03 | 0.90 | 1.03 | 1.07 | 0.80 | 0.15 |

1-C

$60° \leq \zeta < 80°$

$\chi = 0.70 = \text{constant}$

Table A-2

$\chi(\zeta,\theta,\psi)$ factors for the Nimbus III cloud model

2-A

$0° \leq \zeta < 35°$

$\chi = 1.02 = \text{constant}$

2-B

$35° \leq \zeta < 60°$

| θ \ ψ | 0°-30° | 30°-60° | 60°-90° | 90°-120° | 120°-150° | 150°-180° |
|---|---|---|---|---|---|---|
| 0°-10° | 1.00 | 1.00 | 1.00 | 1.00 | 1.00 | 1.00 |
| 10°-20° | 0.93 | 0.93 | 0.93 | 0.95 | 0.95 | 0.95 |
| 20°-30° | 0.90 | 0.90 | 0.93 | 0.93 | 0.93 | 0.90 |
| 30°-40° | 0.87 | 0.87 | 0.90 | 0.93 | 0.88 | 0.83 |
| 40°-50° | 0.83 | 0.83 | 0.85 | 0.85 | 0.80 | 0.70 |
| 50°-60° | 0.75 | 0.75 | 0.76 | 0.76 | 0.68 | 0.53 |

2-C

$60° \leq \zeta < 80°$

| θ \ ψ | 0°-30° | 30°-60° | 60°-90° | 90°-120° | 120°-150° | 150°-180° |
|---|---|---|---|---|---|---|
| 0°-10° | 1.04 | 1.04 | 1.02 | 1.00 | 1.00 | 1.00 |
| 10°-20° | 1.07 | 1.04 | 1.00 | 1.00 | 0.98 | 0.98 |
| 20°-30° | 1.04 | 1.04 | 1.00 | 0.97 | 0.93 | 0.93 |
| 30°-40° | 0.97 | 0.97 | 0.97 | 0.93 | 0.86 | 0.80 |
| 40°-50° | 0.84 | 0.87 | 0.92 | 0.86 | 0.74 | 0.70 |
| 50°-60° | 0.72 | 0.78 | 0.82 | 0.75 | 0.64 | 0.60 |

APPENDIX B.

Standardization and Normalization Procedures

Since measurements of reflected radiance (brightness) are dependent upon the angular conditions of observation, a standardization and/or normalization technique must be applied to the data before valid relative comparisons can be made.

In practice, a time sequence of measurements of a given surface may be taken under different angular conditions because of:

(a) a relatively long elapsed time interval from beginning to end of the sequence (a sensor mounted on a fixed platform), thus changing $\zeta$ and $\psi$ with $\theta$ remaining constant; or,

(b) rapid movement of the instrument (on a satellite or aircraft), thus changing $\theta$ and/or $\psi$ while $\zeta$ remains constant.

Vonder Haar (1969) discusses the proportionality between reflected radiance measurements (also called digital counts or brightness values) and the bi-directional reflectance ($\rho$). Thus, given a digital count, D, at time, t, and point, p, then:

$$D = K_1 V_o = K_1 K_2 N_r(\zeta,\theta,\psi) = K_1 K_2 \rho(\zeta,\theta,\psi) H_i \cos\zeta \quad , \qquad (B1)$$

where $K_1$ and $K_2$ are proportionality constants,

$V_o$ = voltage output from the ATS spin-scan camera,

$N_r$ = measured reflected solar radiance,

$\rho$ = effective bi-directional reflectance of the viewed surface, and

$H_i$ = incident solar irradiance (the solar constant).

Let D' be a digital count from the same cloud or surface at (a) $t + \Delta t$ where p = constant, or (b) $p + \Delta p$ where t = constant. Then:

$$\frac{D}{D'} = \frac{K_1 K_2 \rho H_i \cos \zeta}{K_1 K_2 \rho H_i \cos \zeta'} = \frac{\rho \cos \zeta}{\rho' \cos \zeta'} \quad . \tag{B2}$$

Equation (2) is the general expression used for comparisons between D and D'. In order to express the ratio $\rho/\rho'$, empirical $\chi$ factors were obtained to represent the variation between actual reflectance and Lambert reflectance as discussed in Appendix A.

For the same cloud or surface the directional reflectances (r) are related by:

$$r'(\zeta') = Fr(\zeta) \quad , \tag{B3}$$

where $F = \frac{r'(\zeta')}{r(\zeta=0)} \cdot \frac{r(\zeta=0)}{r(\zeta)} = \frac{r'(\zeta')}{r(\zeta)}$ .

The F factors include the actual directional reflectance [$r(\zeta)$] relative to the directional reflectance at solar noon [$r(\zeta=0)$]. The complete list of model values used is shown in Table B-1.

Since $\chi = \frac{r}{\pi\rho}$ and $\chi' = \frac{r'}{\pi\rho'}$ , then from equation (3)

$$\chi' \pi \rho' = F \chi \pi \rho \quad \text{or,}$$

$$\frac{\rho}{\rho'} = \frac{\chi'}{\chi} \frac{1}{F} = \frac{\chi'}{\chi} \frac{r(\zeta)}{r'(\zeta')} \quad . \tag{B4}$$

Therefore, from equation (2), $\frac{D}{D'} = \frac{\chi' r(\zeta) \cos \zeta}{\chi r'(\zeta') \cos \zeta'}$ or,

$$D = \eta D' = \left[ \frac{\chi'}{\chi} \frac{r(\zeta)}{r'(\zeta')} \frac{\cos \zeta}{\cos \zeta'} \right] D' = \left( \frac{\rho \cos \zeta}{\rho' \cos \zeta'} \right) D' \quad . \tag{B5}$$

Through the proper scaling factor, $\eta$, it is then possible to compare digital values from identical clouds or surfaces (a) taken at different times, but over the same geographical location, or (b) observed at separate locations but at the same time.

Table B-1

Directional reflectance relative to the value at solar zenith angle of zero degrees for the Nimbus III ocean and cloud models

| $\zeta$ | Cos $\zeta$ | Ocean $\left(\frac{r(\zeta)}{r(\zeta=0)}\right)$ | Cloud $\left(\frac{r(\zeta)}{r(\zeta=0)}\right)$ |
|---|---|---|---|
| 0° | 1.00 | 1.00 | 1.00 |
| 18° | 0.95 | 1.00 | 1.00 |
| 26° | 0.90 | 1.00 | 1.00 |
| 32° | 0.85 | 1.00 | 1.00 |
| 37° | 0.80 | 1.00 | 1.05 |
| 41° | 0.75 | 1.03 | 1.10 |
| 45° | 0.70 | 1.10 | 1.14 |
| 49° | 0.65 | 1.20 | 1.18 |
| 53° | 0.60 | 1.30 | 1.22 |
| 57° | 0.55 | 1.40 | 1.28 |
| 60° | 0.50 | 1.60 | 1.32 |
| 63° | 0.45 | 1.80 | 1.38 |
| 66° | 0.40 | 2.00 | 1.42 |
| 69° | 0.35 | 2.20 | 1.48 |
| 72° | 0.30 | 2.50 | 1.52 |
| 75° | 0.25 | 2.80 | 1.55 |
| 78° | 0.20 | 3.10 | 1.58 |
| 81° | 0.15 | 3.40 | 1.60 |
| 84° | 0.10 | 3.70 | 1.60 |
| 87° | 0.05 | 4.00 | 1.60 |

The standardization procedure used this technique to check each ATS picture for unrecorded gain settings. Although the correction factors ($\eta$) computed during standardization were subsequently not used, the stated approach for computing an $\eta$ to account for ocean anisotropy and changes in incident irradiance is theoretically valid.

The normalization procedure used a similar technique to account for cloud anisotropy and changes in incident solar irradiance. Cloud anisotropy, which is the result of the asymmetric bi-directional reflectance pattern of clouds, may account for variations in measured brightness of 1% to 300%. These changes are normalized to a diffuse reflecting Lambert surface via the factor $\chi$. The changes of incident solar irradiance are obtained through the ratio of the cosines of the solar zenith angle. This ratio, in addition to accounting for diurnal solar positions, also compensates for the various solar declinations inherent in the original data. It is the product ($\eta$) of these two correction terms that is then used as a proper scaling factor for digital counts from individual ATS times and locations.

The same reference time and location was used during both the standardization and normalization procedures. This reference was local noon on 15 April and 30°N, local longitude, which enabled a relative minimum of correction factors to be computed. Through these two procedures, it was then possible to compare the ATS digitized pictures on an inter-daily as well as an intra-daily basis.

UNCLASSIFIED

Security Classification

DOCUMENT CONTROL DATA - R & D

*(Security classification of title, body of abstract and indexing annotation must be entered when the overall report is classified)*

1. ORIGINATING ACTIVITY (Corporate author)
Colorado State University
Department of Atmospheric Science
Fort Collins, Colorado 80521

2a. REPORT SECURITY CLASSIFICATION
Unclassified

2b. GROUP
NA

3. REPORT TITLE
VERY SHORT RANGE LOCAL AREA WEATHER FORECASTING USING MEASUREMENTS FROM GEOSYNCHRONOUS METEOROLOGICAL SATELLITES

4. DESCRIPTIVE NOTES *(Type of report and inclusive dates)*
Scientific. Final. 1 November 1970 - 31 January 1972 Approved 2 May 1972

5. AUTHOR(S) *(First name, middle initial, last name)*
Gerald J. Sikula
Thomas H. Vonder Haar

6. REPORT DATE
30 April 1971

7a. TOTAL NO. OF PAGES
73

7b. NO. OF REFS
18

8a. CONTRACT OR GRANT NO.
F19628-71-C-0073

b. PROJECT, TASK, AND WORK UNIT NO.
6698-02-01

c. DOD ELEMENT
62101F

d. DOD SUBELEMENT
686698

9a. ORIGINATOR'S REPORT NUMBER(S)
CSU Atmos. Sci. Paper No.

9b. OTHER REPORT NO(S) *(Any other numbers that may be assigned this report)*
AFCRL-72-0260

10. DISTRIBUTION STATEMENT
A - Approved for public release; distribution unlimited

11. SUPPLEMENTARY NOTES
TECH, OTHER

12. SPONSORING MILITARY ACTIVITY
Air Force Cambridge Research Laboratories (LY)
L. G. Hanscom Field
Bedford, Massachusetts 01730

13. ABSTRACT

Quantitative radiance measurements from NASA's ATS-3 geosynchronous satellite have been used to develop and test a statistical forecast method to predict air terminal weather over the very short range (0-6 hours) time period. Results from more than 800 hourly weather situations at a wide range of U. S. weather stations show that the parameters of ceiling and total opaque cloud cover can be specified or predicted with skill, exceeding persistence forecasts for time periods greater than two hours. Statiscal predictions based on satellite data alone are much better than those based on some 500 mb upper air parameters tested. The potential global applications of the satellite data-based forecasts can apparently be improved by the use of certain criteria, such as region of interest, in developing and applying the multiple regression equation. Considering the present status of objective short range weather forecasting, the initial results of the present study are encouraging.

DD FORM 1 NOV 65 1473

UNCLASSIFIED

Security Classification

| 14. KEY WORDS | LINK A | | LINK B | | LINK C | |
|---|---|---|---|---|---|---|
| | ROLE | WT | ROLE | WT | ROLE | WT |
| Geosynchronous Satellite Data | | | | | | |
| Meteorology | | | | | | |
| Short Range Forecasting | | | | | | |
| Ceiling-Visibility | | | | | | |
| Radiation Measurements | | | | | | |
| Cloud Observations | | | | | | |

181. Real Time Direct Read-Out Satellite Support to Meteorological Research Programs and Forecasting Units. Miller, Harvey Joe. Master's Thesis, sponsored by AFIT, March 1972.

182. Structure in Dynamics of the Hurricane's Inner Core Region. Dennis J. Shea's Master's Thesis, sponsored by NOAA Grant N22-65-72 (G) and NSF Grant #19937, March, 1972.

183. Cyclones and the Atmospheric Water Cycle - A Survey of Research Objectives. H. Riehl and J. L. Rasmussen, 1972.

184. Measurements of the Energy Exchange between Earth and Space from Satellites during the 1960's. T. H. Vonder Haar and E. Raschke, sponsored by NASA Grant No. NGR-06-002-102. April, 1972.

181. Real Time Direct Read-Out Satellite Support to Meteorological Research Programs and Forecasting Units. Miller, Harvey Joe. Master's Thesis, sponsored by AFIT, March 1972.

182. Structure in Dynamics of the Hurricane's Inner Core Region. Dennis J. Shea's Master's Thesis, sponsored by NOAA Grant N22-65-72 (G) and NSF Grant #19937, March, 1972.

183. Cyclones and the Atmospheric Water Cycle - A Survey of Research Objectives. H. Riehl and J. L. Rasmussen, 1972.

184. Measurements of the Energy Exchange between Earth and Space from Satellites during the 1960's. T. H. Vonder Haar and E. Raschke, sponsored by NASA Grant No. NGR-06-002-102. April, 1972.